Continuous Variable in Quantum Networking.

By

Sundus Abrar

Fall-2021-MSPhy 00000365263 School of Natural Science

Supervisor

Dr. Aeysha Khalique

Department of Physics

A thesis submitted in partial fulfillment of the requirements for the degree of Master of Science in Physics (MSPHY)

In

School of Natural Science (SNS),

National University of Sciences and Technology (NUST),

Islamabad, Pakistan.

(August 2024)

THESIS ACCEPTANCE CERTIFICATE

Certified that final copy of MS thesis written by **Sundus Abrar** (Registration No. **00000365263)**, of **School of Natural Sciences** has been vetted by undersigned, found complete in all respects as per NUST statutes/regulations, is free of plagiarism, errors, and mistakes and is accepted as partial fulfillment for award of MS/M.Phil degree. It is further certified that necessary amendments as pointed out by GEC members and external examiner of the scholar have also been incorporated in the said thesis.

Signature: _____

Name of Supervisor: Dr. Aeysha Khalique_____

Date: __27 | 9 | 24_____

Signature (HoD): _____

Date: _____27-09-2024_____

Signature (Dean/Principal): _____

Date: __27.09.2024_____

National University of Sciences & Technology

MS THESIS WORK

We hereby recommend that the dissertation prepared under our supervision by: Sundus Abrar, Regn No. 00000365263 Titled: Continues Variable in Quantum Networking be Accepted in partial fulfillment of the requirements for the award of **MS** degree.

Examination Committee Members

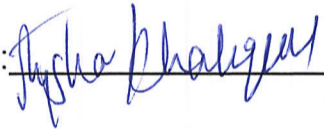1. Name: DR. MUHAMMAD ALI PARACHA   Signature:

2. Name: DR. SAADI ISHAQ   Signature:

Supervisor's Name DR. AEYSHA KHALIQUE   Signature:

_____
Head of Department

27-09-2024
Date

COUNTERSINGED

Date: 27-09-2024

Dean/Principal

Dedication

This thesis is dedicated to my dear friends, whose unwavering support and companionship have been a source of strength throughout this journey, and my siblings, who have always stood by me, providing encouragement and understanding every step of the way. Most especially, to my parents, with deepest gratitude to my mother. Her boundless love, sacrifice, and belief in my dreams have made this achievement possible. This work is as much hers as it is mine.

Certificate of Originality

I hereby declare that this submission is my own work and to the best of my knowledge it contains no materials previously published or written by another person, nor material which to a substantial extent has been accepted for the award of any degree or diploma at adviserAffiliation at school or at any other educational institute, except where due acknowledgement has been made in the thesis. Any contribution made to the research by others, with whom I have worked at school or elsewhere, is explicitly acknowledged in the thesis. I also declare that the intellectual content of this thesis is the product of my own work, except for the assistance from others in the project's design and conception or in style, presentation and linguistics which has been acknowledged.

Author Name: **author**

Signature: _____

Acknowledgments

I would like to start by thanking my supervisor, **Dr. Aeysha Khalique**, for her guidance, support, and valuable feedback throughout my research. Her help has been crucial in completing this thesis. I am also very thankful to **Farsad Ahmed** for his assistance and support during this journey. His help made a big difference. Lastly, I want to express my heartfelt thanks to my best friend, **Muhammad Kumail Haider**. He has been there for me every step of the way, offering encouragement and help whenever I needed it.

.

author

Abstract

Quantum information science takes advantage of the curious properties of quantum mechanics in order to design protocols for information processing that lie beyond the capability of their classical counterparts. This review focuses on continuous-variable graph states for regular network structures with an eye on cost as a figure of merit quantifying both the required squeezing and the number of needed squeezed modes to build up the network. An analytic formula has been deduced for the experimental resources needed to realize those graph states; it is shown that scaling of squeezing cost with network size depends directly on its topology. In addition, the effect of introducing loss is investigated, which further decreases the squeezing cost, and the performance of the squeezing is strongly dependent on both the structure and surroundings of the network. These findings can provide important insight into the design and optimization of quantum networks.

Thesis Outline

Chapter 1 introduces basic quantum mechanics, focusing on concepts that most distinguish quantum mechanics from classical mechanics. Specific topics range from qubits, including quantum gates and operations, to the use of discrete variables in quantum networking, and a general introduction to continuous variables. Continuous variables are put into perspective with regard to their advantageous use compared to discrete variables in some quantum information tasks.

Chapter 2 is dedicated to Gaussian states, which constitute an important ingredient of continuous variable quantum information. The measurement techniques on Gaussian states treated in the text include also partial measurements. Then, the text treats coherent states and their relation to the displaced vacuum state. Finally, a detailed treatment of squeezed vacuum states, single and two-mode-and their relevance in quantum information processing, as well as the squeezing that affects resource requirements is performed.

Chapter 3 goes into the details of the realm of continuous variables, concerning mathematical representation and issues related to operations. Continuous variable quantum information processing: Covariance matrices for vacuum, coherent, single-mode squeezed, and two-mode squeezed vacuum states are derived. Gaussian quantum operations are described and effects of transmittance and noise on continuous variable quantum systems are looked upon.

Chapter 4 expands on Gaussian networks, analyzing different types of network graphs, such as linear, cycle, wheel, star, complete, and grid graphs. It explores the role of graph states in quantum networks and provides a resource theory perspective on quantifying squeezing. The chapter also investigates network generation via squeezing cost and models Gaussian quantum channels, comparing squeezing in pure loss channels with different network configurations. In chapter 5, the results of the research are presented and discussed. It includes an analysis of the squeezing cost across various network types, focusing on nodes and modes. The chapter

also examines the impact of noise on squeezing cost, providing insights into how noise affects different network configurations and quantum modes. This section offers a detailed discussion of the findings and their implications for quantum information processing.

Contents

List of Figures

Introduction to Quantum Information

1.1 Overview of Quantum Mechanics

In the world of quantum mechanics, particles do not behave as might be reasonably expected from our greater life experiences. Whereas in the classical world, objects have definite positions and trace out predictable paths, in the quantum world the rules that govern the motion of objects are few in number but many of them run completely against our intuition.

With superposition, one particle-a single electron, for example be in more than one state at a single instant. Think about that: a very small particle being in two places at once or spinning both clockwise and counterclockwise at the same time. This is no mere theoretical fancy but a real phenomenon illustrated in innumerable experiments. It's one of the chief features giving quantum systems their extraordinary power.

Entanglement is another conception of quantum mechanics. In such a situation, two particles become so intertwined in their fates, that the instant state of one depends on the instant state of another, no matter how far they are from each other. These two phenomena superposition and entanglement are not abstract creations but the very pillars on which quantum information science has been built. In this field, we avail the aforementioned quantum principles to manipulate and transit information in manners impossible in the classical world.

1.2 Classical vs Quantum Mechanics

Having established the foundational principles of quantum mechanics, we can now explore how these principles differentiate quantum information from classical information.

1.2.1 Classical Mechanics

The bit is a binary unit of information; it is, in fact, the basic unit of information in a classical setting. The bits can classically take on one of two states: 0 and 1. These bits form the very basics of all classical information processing systems, which include computers, smartphones, and communication networks. Classical gates, such as AND, OR, and NOT, manipulate these bits according to well-defined rules. The outcome of any classical computation is deterministic, meaning that the same input will always produce the same output.

1.2.2 Quantum Mechanics

Quantum information, in particular, resides in qubits, which, as we have seen, may exist in superpositions of states. In fact, this ability to be in more than one state at the same time endows quantum computers with their exponential advantage for some types of computations.

There is also no classical analog to some of the quantum gates acting on qubits. As an example, the Hadamard gate will transform the basis states $|0\rangle$ and $|1\rangle$ into equal superpositions:

$$H|0\rangle = \frac{|0\rangle + |1\rangle}{\sqrt{2}}, \quad H|1\rangle = \frac{|0\rangle - |1\rangle}{\sqrt{2}}. \tag{1.2.1}$$

Consequently, the ability to generate and manage these superpositions and entangled states enables quantum computers to solve specific problems much faster, exponentially so, compared to classical computers: factoring enormous numbers.

1.3 Qubits: The building blocks of Quantum information

1.3.1 The concept of Qubit

A qubit represents the quantum counterpart of the classical bit but with a great deal more various behavior: While a classical bit can be 0 or 1, a qubit can exist in a superposition of both states. [9]. The general state of a qubit is written as:

$$|\psi\rangle = \alpha|0\rangle + \beta|1\rangle. \tag{1.3.1}$$

Here, α and β are complex coefficients that determine the likelihood of the qubit being measured in either the $|0\rangle$ or $|1\rangle$ state. The power of a qubit comes from the fact that it can represent both

possibilities simultaneously, unlike a classical bit, which is strictly one or the other.

1.3.2 Quantum gates and operation

Quantum gates are the quantum version of classical logic gates - they operate on qubits. They are unitary matrices applied to the qubits in order for the states to evolve.

The most basic quantum gate is the so-called Hadamard gate H; it generates a superposition out of a basis state:

$$H = \frac{1}{\sqrt{2}} \begin{pmatrix} 1 & 1 \\ 1 & -1 \end{pmatrix}. \tag{1.3.2}$$

Applying the Hadamard gate to the $|0\rangle$ state creates an equal superposition of $|0\rangle$ and $|1\rangle$:

$$H|0\rangle = \frac{|0\rangle + |1\rangle}{\sqrt{2}}. \tag{1.3.3}$$

Another of the very useful gates is the Controlled-NOT (CNOT) gate. This gate acts on two qubits-flipping the second qubit, the target, if and only if the first qubit, the control, is in the state $|1\rangle$. The preparation of entangled states is central to many of the quantum computing and communication protocols.

1.4 Discrete variable in quantum Network

It is important to note, as we shall now consider quantum networks more explicitly, that the role of discrete variables, and in particular, qubits plays an important part. Discrete variables are usually understood as quantum systems with only a finite number of possible states. Qubits, which can be in states $|0\rangle$ or $|1\rangle$ (or superpositions thereof), are the most common examples of discrete variables in quantum computing. In quantum networks, these discrete variables are used to encode and transmit information between different nodes.

However, while discrete variables are powerful, they are not without limitations. For example, creating and maintaining entangled states of many qubits can be challenging due to decoherence and noise, which can degrade the quantum information over time.

Quantum networks are systems that use quantum entanglement to connect qubits over a distance to be applied for secure information transmission and accomplished distributed quantum

computation [10]. Qubits, in quantum networks, represent the usual information carriers, and protocols such as Quantum Key Distribution ensure data security.

While discrete variables have been central to the development of early quantum networks, the challenges associated with scaling up these networks have led researchers to explore alternative approaches, such as continuous variables, which offer different advantages in terms of scalability and noise resistance.

1.5 Introduction to continuous variable

1.5.1 Discrete vs continuous variable

As we have seen, discrete variables like qubits are the foundation of many quantum information protocols. However, there are scenarios where discrete variables might not be the most efficient or practical choice. This is where continuous variables come into play.

Continuous variables are parameters of a quantum system to encode information, such as the amplitude and phase of electromagnetic fields. [6], unlike qubits, which have distinct states, continuous variable systems can take on a continuous range of values, offering new possibilities for quantum information processing.

1.5.2 The concept of continuous variable

Continuous-variable quantum systems encode information in light quadratures corresponding to the position and momentum of the quantum state. Such variables can take any value on a continuum, rather than just discrete states as is the case for qubits.

As an example, a quantum harmonic oscillator such as a mode of the electromagnetic field may be described in terms of the position X and momentum P quadratures [7], where coherent states and squeezed states represent the most well-known Gaussian states in continuous variable systems.

1.5.3 Quantum states in Continuous variable

Coherent states, which are often represented as $|\alpha\rangle$, where α is a complex number, are the closest quantum analogs to classical states of light. They are eigenstates of the annihilation

operator $\hat{a}$, satisfying: Coherent states, usually denoted by $|\alpha\rangle$, where α is a complex number, are the closest quantum analogs to the classical states of light. They are eigenstates of the annihilation operator$\hat{a}$,obeying

$$\hat{a}|\alpha\rangle = \alpha|\alpha\rangle. \tag{1.5.1}$$

Another important class of states in continuous variable systems is squeezed states. In this state, the uncertainty of one quadrature (for example, position) is reduced at the expense of increased uncertainty of the conjugate quadrature (for example, momentum):

$$\Delta X \Delta P \geq \frac{\hbar}{2}, \tag{1.5.2}$$

If, in the squeezed state, the uncertainty of the position quadrature X decreases below the level of the vacuum state, then the uncertainty of the momentum quadrature P will grow correspondingly. Squeezed states play an important role in enhancing measurement precision in quantum metrology and offer improved performances in quantum communication protocols.

1.6 Why prefer CV over DV

Continuous variables offer several advantages as information carriers over discrete variables:

- **Infinite Dimensionality**: Continuous variables provide the capability to extend systems into infinite dimensions, something that discrete variables cannot achieve.

- **Unconditional Implementation**: Continuous variables can be implemented consistently without needing specific conditions. While discrete variables might be more efficient in some scenarios, they lack the assurance of successful implementation every time.

- **Error Tolerance**: Continuous variables are more robust against errors than discrete variables, such as qubits. Qubits can be easily flipped from $|0\rangle$ to $|1\rangle$ or vice versa due to channel defects or environmental noise, which can significantly alter the system. Continuous variables, however, are less susceptible to such errors.

Gaussian States

A Gaussian state is defined as any state that can be completely characterized by its mean and variance, denoted as

$$\hat{\rho} = \hat{\rho}(\bar{x}, V). \tag{2.0.1}$$

Since their Wigner function is a Gaussian distribution, these states remain Gaussian under Gaussian operations. [23]. Gaussian states in the framework of quantum physics must not break the uncertainty principle. This comes after:

$$\langle \hat{x} \rangle = \text{Tr}(\hat{x}\rho), \qquad V_{ij} = \frac{1}{2} \langle \{ \Delta \hat{x}_i \Delta \hat{x}_j \} \rangle \quad \hat{x} \in \{\hat{q}, \hat{p}\}. \tag{2.0.2}$$

such that;

$$\Sigma + i\Omega \geq 0, \tag{2.0.3}$$

where Ω is given as

$$\Omega = \begin{pmatrix} 0 & 1 \\ -1 & 0 \end{pmatrix}. \tag{2.0.4}$$

and Σ represents the Covariance matrix which has the following structure;

$$\Sigma = \begin{pmatrix} V(\hat{q}) & C(\hat{q}, \hat{p}) \\ C(\hat{q}, \hat{p}) & V(\hat{p}) \end{pmatrix}. \tag{2.0.5}$$

The variance, denoted as V, of the quadrature operators $(\hat{q})$ and $(\hat{p})$ in Gaussian states is a real positive value that is consistently larger than or equal to 1. We extract the uncertainty relation from the covariance matrix's diagonal entries.

$$V(\hat{q})V(\hat{p}) \geq 1, \tag{2.0.6}$$

This relation ensures that Gaussian states comply with the uncertainty principle [5]. The covariance C between respective quadratures is crucial in CV QKD. Covariance is a measure of how

much two random variables change together. If the covariance between two quadratures is zero, they are uncorrelated and hence separable. Generally, covariance can be negative and positive indicating inverse correlation, where an increase in one quadrature results in a decrease in the other while positive covariance indicates direct correlation, where an increase in one quadrature increases the other. Entanglement, a necessary feature for quantum communication, requires non-separability and thus non-zero covariance. In a single-mode Gaussian system, quadratures are always uncorrelated because they are orthogonal, resulting in zero covariance. This orthogonality means that knowing one quadrature gives no information about its conjugate. Correlations emerge in multi-mode states. For a two-mode state, the probability distribution is highest at zero and decays exponentially as we move away from the center. The form of a two-mode Gaussian state can illustrate this concept. In the context of quantum mechanics, Gaussian states must adhere to the uncertainty principle, which follows from the covariance relations. In a two-mode system, the covariance term $C(\hat{q}_1, \hat{q}_2)$ not necessarily zero. This non-zero covariance indicates a correlation between mode-1 and mode-2, such that any change in $(\hat{q})$ affects the distribution of $(\hat{p})$.

2.1 Measuring Gaussian States

In quantum communication, continuous variable (CV) systems utilize the quadrature of light (position and momentum) to encode and transmit information. This method leverages the benefits of existing telecommunication technologies, making it highly practical for real-world applications. Key components in CV quantum communication include single photon detectors and homodyne detectors. Detecting a single photon directly is challenging due to the extremely low signal strength. An indirect method in which when a photon strikes a photocathode, it ejects an electron. This electron is then amplified through a series of dynodes. Each dynode multiplies the incoming electrons, exponentially increasing the signal strength. This method gives protection against multi-photon signals. The downside of this detector is that the photocathode may not eject an electron every time, even when it does the electron may not always land on the dynode. This heavily affects the efficiency of a single photon detector. The amplified signal is then measured as an electrical current using standard electronic devices. However, homodyne detection is a technique that mixes the incoming quantum signal with a classical signal (local oscillator) to measure the quadrature of light. The setup includes A classical signal whose phase can be adjusted to choose the quadrature to be measured (position or momentum). By controlling the
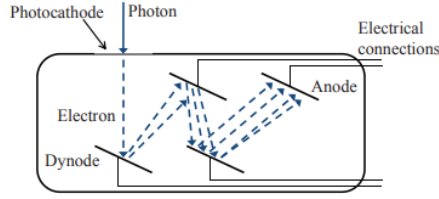
Figure 2.1: A single photon is converted into an electrical signal, which is then amplified through multiple dynodes until the resulting current is strong enough to be measured using standard electrical devices.

[11]

phase, specific quadratures are amplified, making them easier to measure. homodyne detection amplifies the quantum signal, making it detectable with simple photodetectors. To understand the mathematics of this process, we first introduce coherent states of light. The annihilation operator is given as

$$\hat{a} = \frac{1}{2}(\hat{q} + i\hat{p}), \tag{2.1.1}$$

and the classical field operator is given as

$$\alpha_{LO} = q + ip = |\alpha_{LO}|e^{i\theta}, \tag{2.1.2}$$

LO represents the local operator. Let $\hat{a}$ and α_{LO} each enter a balanced beam splitter, represented by

$$BS = \frac{1}{\sqrt{2}} \begin{pmatrix} 1 & 1 \\ 1 & -1 \end{pmatrix}, \tag{2.1.3}$$

The action of a beamsplitter on the quantum field $\hat{b}$ and the classical field β_{LO} is represented as follows:

$$BS \begin{pmatrix} \hat{b} \\ \beta_{LO} \end{pmatrix} = \begin{pmatrix} \frac{1}{\sqrt{2}}(\hat{b} + \beta_{LO}) \\ \frac{1}{\sqrt{2}}(\hat{b} - \beta_{LO}) \end{pmatrix} = \begin{pmatrix} \hat{b}_1 \\ \hat{b}_2 \end{pmatrix}. \tag{2.1.4}$$

Here, $\hat{b}_1$ and $\hat{b}_2$ are the annihilation operators corresponding to the two output ports of the beamsplitter. The photon-number operators for each output can be expressed as:

$$\hat{m}_1 = \hat{b}_1^\dagger \hat{b}_1 = \frac{1}{2}(\hat{b}^\dagger + \beta_{LO}^*)(\hat{b} + \beta_{LO}) = \frac{1}{2}(\hat{b}^\dagger \hat{b} + \beta_{LO}^*\beta_{LO} + \beta_{LO}\hat{b}^\dagger + \beta_{LO}^*\hat{b}), \tag{2.1.5}$$

$$\hat{m}_2 = \hat{b}_2^\dagger \hat{b}_2 = \frac{1}{2}(\hat{b}^\dagger - \beta_{LO}^*)(\hat{b} - \beta_{LO}) = \frac{1}{2}(\hat{b}^\dagger \hat{b} + \beta_{LO}^*\beta_{LO} - \beta_{LO}\hat{b}^\dagger - \beta_{LO}^*\hat{b}), \tag{2.1.6}$$

8

Subtracting the two gives the photon-number difference operator:

$$\hat{m} = \hat{m}_1 - \hat{m}_2 = \beta_{LO}\hat{b}^\dagger + \beta_{LO}^*\hat{b} \qquad (2.1.7)$$

Substituting Eqn. 2.1.1 in Eqn. 2.1.7 we get

$$\hat{m} = |\beta_{LO}|(\hat{b}^\dagger e^{i\phi} + \hat{b}e^{-i\phi}) = |\beta_{LO}|\frac{1}{2}([\hat{x} - i\hat{y}]e^{i\phi} + [\hat{x} + i\hat{p}]e^{-i\phi}), \qquad (2.1.8)$$

$$= |\beta_{LO}|\frac{1}{2}(\hat{x}[e^{i\phi} + e^{-i\phi}] + i\hat{p}[-e^{i\phi} + e^{-i\phi}]), \qquad (2.1.9)$$

Since $e^{i\phi} + e^{-i\phi} = 2\cos\phi$ and $e^{i\phi} - e^{-i\phi} = -2i\sin\phi$, we get:

$$\hat{m} = |\beta_{LO}|(\hat{x}\cos\phi + \hat{p}\sin\phi). \qquad (2.1.10)$$

The phase difference between the incoming signal and the classical signal is denoted by ϕ. It is equivalent to the local oscillator's phase in the context of homodyne detectors. We can improve the quadrature we plan to measure by changing this phase.. For instance, setting $\phi = 0$ allows us to measure position, while $\phi = \pi/2$ enables us to measure momentum. Notably, the number-difference operator, being proportional to the photodetector current, indicates that a current is detected only when we amplify the correct quadrature.

Another detection method, known as heterodyne detection or dual-homodyne detection, involves splitting the incoming signal into two equal parts using a balanced beamsplitter. One part is then sent to a homodyne detector with $\phi = 0$, while the other part goes to a homodyne detector with $\phi = \pi/2$.

Heterodyne detection offers the advantage of measuring both quadratures simultaneously. This capability is valuable for estimating channel parameters as it reduces Eve's information [30, 20]. However, this method introduces additional noise due to signal amplitude reduction from splitting. Considering that measuring signals inherently have a noise level of 1 SNU (Standard Noise Units) due to the uncertainty principle, measuring both quadratures leads to twice the intrinsic noise.

2.1.1 Partial Measurements

In Gaussian quantum information processing, we work with the covariance matrix. A partial measurement on this covariance matrix influences the entire system as described below.

Partial Homodyne Transformation:

$$V = A - C\left(\Pi_{q,p}B\Pi_{q,p}\right)^{-1}C^T.$$ (2.1.11)

Partial Heterodyne Transformation:

$$V = A - C\left(B + I\right)^{-1}C^T.$$ (2.1.12)

Given that:

$$V = \begin{pmatrix} A_{n\times n} & C_{n\times 2} \\ C_{2\times n} & B_{2\times 2} \end{pmatrix}, \qquad \Pi_q = \begin{pmatrix} 1 & 0 \\ 0 & 0 \end{pmatrix}, \qquad \Pi_p = \begin{pmatrix} 0 & 0 \\ 0 & 1 \end{pmatrix}, \qquad I = \begin{pmatrix} 1 & 0 \\ 0 & 1 \end{pmatrix}.$$ (2.1.13)

Here, V represents the covariance matrix that undergoes a partial transformation. The projective matrix Π depends on the choice of quadrature measured, and I is the identity matrix. The term $\left(\Pi_{q,p}B\Pi_{q,p}\right)^{-1}$ is not a standard inverse but rather a pseudoinverse, specifically known as the Moore-Penrose inverse [14].

The dimension of B is always 2×2. This is because each partial measurement is performed on one mode, which consists of the variances of q, p, and their covariance. It is important to note that if a protocol involves multiple partial measurements, they should be executed sequentially, as one partial measurement can impact the result of another. When a partial measurement is performed on this system, the transformation affects the entire covariance matrix V. The dimension constraint on B ensures that each mode is accurately represented by its variances and covariances. Sequential execution of multiple partial measurements ensures that the results are not skewed by the interdependencies of the measurements.

2.2   Coherent State

When the position (ΔX) and momentum (ΔP) uncertainties are multiplied and the result is $\Delta X = \Delta P = \frac{1}{2}$, the coherent state of the harmonic oscillator is defined as a unique quantum state that preserves minimum uncertainty. This highlights the significance of coherent states in quantum optics and quantum physics. The eigenstate of the annihilation operator a, a basic operator in the quantum harmonic oscillator, is defined mathematically as the coherent state $|\alpha\rangle$ [18]. This means that applying the annihilation operator to a coherent state results in the same state scaled by the eigenvalue α:

$$a|\alpha\rangle = \alpha|\alpha\rangle.$$ (2.2.1)
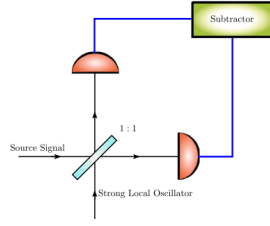
Figure 2.2: Homodyne detection
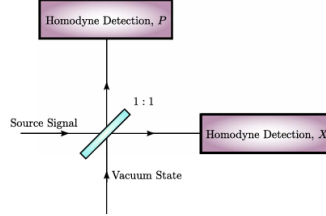
Figure 2.3: Hetrodyne detection

Figure 2.4: Partial measurement using Homodyne and Heterodyne detection

[19]

Similar results are obtained by treating the conjugate of the coherent state as the adjoint (creation) operator $a^\dagger$.

$$\langle \alpha | a^\dagger = \alpha \langle \alpha |. \tag{2.2.2}$$

The amplitude of the coherent state is represented by the parameter α, which may be a complex value. The number (Fock) states $|n\rangle$ can be used to expand the coherent state $|\alpha\rangle$ as follows.s:

$$|\alpha\rangle = e^{-|\alpha|^2/2} \sum_{n=0}^{\infty} \frac{\alpha^n}{\sqrt{n!}} |n\rangle, \tag{2.2.3}$$

where $|n\rangle = \frac{(a^\dagger)^n}{\sqrt{n!}} |0\rangle$ is the n-th number state and $|0\rangle$ is the vacuum state. Several important properties of coherent states are explained below: The average number of photons in a coherent state $|\alpha\rangle$ is given by the expectation value:

$$\langle \alpha | a^\dagger a | \alpha \rangle = |\alpha|^2. \tag{2.2.4}$$

This indicates that the number of photons follow a Poisson distribution. The probability $p(n)$ of finding exactly n photons in the coherent state is:

$$p(n) = |\langle n | \alpha \rangle|^2 = \frac{\langle n \rangle^n e^{-\langle n \rangle}}{n!}, \tag{2.2.5}$$

where $\langle n \rangle = |\alpha|^2$. Coherent states are also known as minimum uncertainty states because they
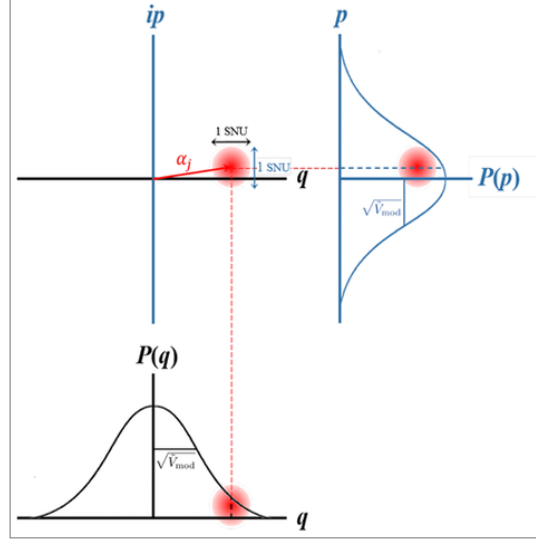
Figure 2.5: Phase space representation of Gaussian modulated coherent state $|\alpha_j\rangle$ with a variance of 1 shot noise unit and a non-zero mean value [25]

satisfy the equality in the Heisenberg uncertainty principle:

$$\Delta X \Delta P = \frac{\hbar}{2}. \tag{2.2.6}$$

This indicates that location and momentum errors are as narrow as permitted by quantum mechanics. The quantum harmonic oscillator's Hilbert space is entirely composed of coherent states. This consistency can be stated as follows:

$$\int |\alpha\rangle\langle\alpha| d^2\alpha = 1, \tag{2.2.7}$$

where $d^2\alpha$ denotes integration over the complex plane of the parameter α.

2.3 Displaced Vacuum state and Coherent State

The relationship between a coherent state $|\alpha\rangle$ and the displacement operator $D(\alpha)$ can be expressed as

$$|\alpha\rangle = D(\alpha)|0\rangle. \tag{2.3.1}$$

. The displacement operator $D(\alpha)$ is defined as

$$D(\alpha) = e^{-\frac{|\alpha|^2}{2}} e^{\alpha a^\dagger} e^{-\alpha^* a}, \tag{2.3.2}$$

where $a^\dagger$ and a are the creation and annihilation operators, respectively. This operator acts on the vacuum state $|0\rangle$, resulting in the coherent state $|\alpha\rangle$. Essentially, the coherent state

is a displaced vacuum state, where the displacement is determined by the complex parameter α. This relationship highlights the role of the displacement operator in generating coherent states from the vacuum state, providing a fundamental link between the two states in quantum mechanics [25].

2.4 Squeezed Vacuum State

In squeezed states, electromagnetic fields have less noise than in the vacuum state. In other words, light in a such state has less noise, than when no light at all is present. Squeezed states can be conceptualized by using a harmonic oscillator for an analogy.

According to quantum physics, the electromagnetic field's lowest energy is represented by the vacuum state. But because of the Heisenberg uncertainty principle, there is always some quantum noise in every mode. Squeezed states, on the other hand, are specially prepared states where this noise is redistributed. In these states, the noise or uncertainty in one quadrature of the field, such as position or momentum for a harmonic oscillator, is reduced below the level of the vacuum state. The noise in the conjugate variable increases to keep the overall uncertainty consistent with the uncertainty principle.

2.4.1 Single mode Squeezed Vacuum State

A system with two quadratures, position, and momentum, has wave functions for a squeezing factor R as follows: In the position basis:

$$\psi_R(X) = \sqrt{\frac{R}{\pi^{1/2}}} e^{-\frac{(RX)^2}{2}}, \tag{2.4.1}$$

On the momentum basis:

$$\psi_R(P) = \sqrt{\frac{1}{R\pi^{1/2}}} e^{-\frac{(P/R)^2}{2}}, \tag{2.4.2}$$

The variances of the canonical observables are given by:

$$\langle (\Delta X)^2 \rangle = \frac{1}{2R^2}, \tag{2.4.3}$$

$$\langle (\Delta P)^2 \rangle = \frac{R^2}{2}, \tag{2.4.4}$$

There are two scenarios for squeezing: if $R > 1$, the variance in position is less than that of the vacuum state, resulting in a position-squeezed state [2]. Conversely, if $R < 1$, the state
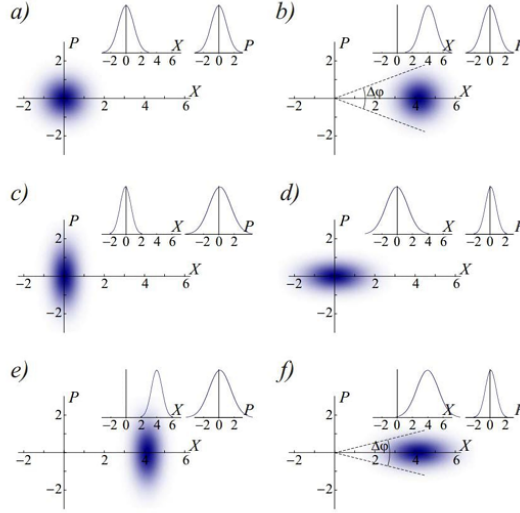
Figure 2.6: Wigner functions for various single-oscillator states: (a) Vacuum state, (b) Coherent state, (c, d) Position and momentum squeezed vacuum states, (e, f) Position and momentum compressed coherent states with real amplitude.

[1]

becomes momentum-squeezed due to the reduced variance in momentum. According to the Heisenberg uncertainty principle, two quadratures that are not orthogonal cannot be measured simultaneously. The relationship between their variances is given by:

$$\langle (\Delta X)^2 \rangle \langle (\Delta P)^2 \rangle = \frac{1}{4}. \tag{2.4.5}$$

The squeezing function can be effectively analyzed through the Wigner function, which is the quantum equivalent of a phase space probability density. The Wigner function provides a complete representation of the quantum state, capturing both position and momentum distributions.

2.4.2 Two modes Squeezed vacuum State

In both theoretical and experimental contexts, a Two-Mode Squeezed Vacuum State (TMSVS) shares similarities with a Single-Mode Squeezed Vacuum State (SMSVS), yet they exhibit distinct characteristics. A TMSVS, also known as a twin-beam state, describes a condition where two mechanical and electromagnetic oscillators are phase-synchronized [1]. The wave functions of TMSVS in the position is,

$$\psi_R(X_a, X_b) = \frac{1}{\sqrt{\pi}} e^{-\frac{R^2(X_a - X_b)^2}{4}} e^{-\frac{(X_a + X_b)^2}{4R^2}}, \tag{2.4.6}$$

14

and in the momentum basis is

$$\psi_R(P_a, P_b) = \frac{1}{\sqrt{\pi}} e^{-\frac{R^2(P_a+P_b)^2}{4}} e^{-\frac{(P_a-P_b)^2}{4R^2}},$$

(2.4.7)

The variances of the quadratures are:

$$\langle(\Delta X_a)^2\rangle = \langle(\Delta X_b)^2\rangle = \langle(\Delta P_a)^2\rangle = \langle(\Delta P_b)^2\rangle = \frac{1+R^4}{4R^2}.$$

(2.4.8)

For $R = 1$, the state is a vacuum state, while for $R \neq 1$, squeezing occurs. As R increases, the uncertainty in the quadratures also increases.
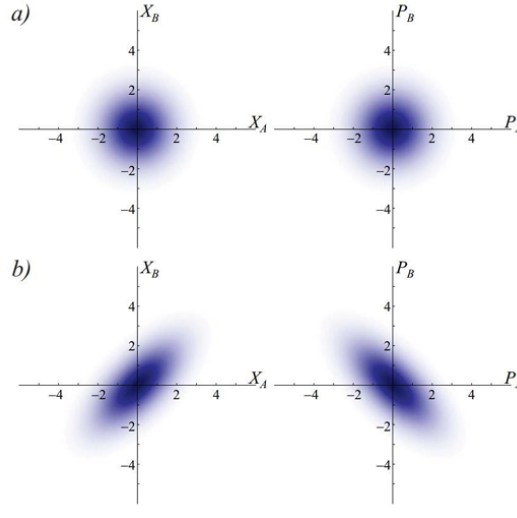
Figure 2.7: Wave functions of two-mode position and momentum squeezed states: (a) Uncorrelated vacuum state in both position and momentum bases, (b) Two-mode squeezed state exceeding the standard quantum limit, characterized by correlated position observables and anti-correlated momentum observables.

[1]

2.5   Contribution of squeezing in Quantum Information

Many fields of quantum information greatly benefit from the work of squeezers. A significant source of entanglement in many quantum information processing systems is the squeezed states, specifically the two-mode squeezed vacuum state. Then, such states are required for quantum teleportation, entanglement swapping, and key distribution mechanisms.

Squeezed states have been studied and applied to the deepening of understanding with regards to the key process of generating entangled photon pairs, including polarization-entangled pho-

tons, known as parametric down-conversion. These are fundamental resources for quantum communication and quantum cryptography.

Squeezed states are fundamental CV quantum operators that will extend the range and efficiency of quantum communication. Two-mode squeezing combined with techniques like quantum teleportation can extend the distances in quantum communications by many orders of magnitude.

Introduction to Continuous Variable in Quantum Information

Contemporary research in quantum information is progressing along two primary streams: one focuses on information processing using discrete variables (qubits), and the other utilizes continuous variable (CV) Gaussian states. A coherent state or a compressed vacuum state can both be Gaussian states.

Gaussian states are easily generated in continuous variable systems with common optical technologies like lasers. Moreover, optical components such as homodyne detectors, beam splitters, and amplifiers can be used to readily modify these states. Researchers have started adjusting the momentum and position CV states of mechanical oscillators in the last several years. [17].

In CV systems, the two quadratures of the amplitude of a mode of an electromagnetic field serve as the canonical variables. These quadratures function as the position ($\hat{x}$) and momentum ($\hat{p}$) operators [3], defined as follows:

$$\hat{x} = \sqrt{\frac{\hbar}{2\omega}}(\hat{a} + \hat{a}^\dagger), \tag{3.0.1}$$

$$\hat{p} = -i\sqrt{\frac{\hbar\omega}{2}}(\hat{a} - \hat{a}^\dagger), \tag{3.0.2}$$

.

3.1 Covariance Matrices of Different Gaussian States

A covariance matrix is a square matrix that summarizes the covariance between the pair of elements of a random vector. The variances of the individual elements correspond to the diagonal entries of this matrix, which actually denotes the self-covariance. In the theory of probability and statistics, the variances of random points in two-dimensional space cannot be represented by one number but instead by a 2×2 matrix to fully describe the situation.

Variance pertains to the change in a single random variable, while covariance represents the combined change in two random variables. In a quantum mechanical setting, the covariance matrix provides an exact characterization of the two-point correlations. Below are the covariance matrices for some important states.

3.1.1 Vacuum State

The density matrix for the vacuum state is given by:

$$\rho = |0\rangle\langle 0|. \tag{3.1.1}$$

The elements of the covariance matrix are defined as:

$$\gamma_{ij} = \text{Tr}\left[\rho\frac{1}{2}\left(\Delta\hat{X}_i\Delta\hat{X}_j + \Delta\hat{X}_j\Delta\hat{X}_i\right)\right], \tag{3.1.2}$$

To find the first element of the covariance matrix, we have:

$$\gamma_{11} = \text{Tr}\left[\rho\frac{1}{2}\left(\Delta\hat{X}_1\Delta\hat{X}_1 + \Delta\hat{X}_1\Delta\hat{X}_1\right)\right], \tag{3.1.3}$$

Simplifying, we get:

$$\gamma_{11} = \text{Tr}\left[\rho\left(\Delta\hat{X}_1^2\right)\right], \tag{3.1.4}$$

Using the definition of $\Delta\hat{X}_1$, we expand:

$$\gamma_{11} = \text{Tr}\left[\rho\left(\hat{X}_1^2 - 2\hat{X}_1\langle\hat{X}_1\rangle + \langle\hat{X}_1\rangle^2\right)\right], \tag{3.1.5}$$

Assuming a zero mean value, $\langle\hat{X}_1\rangle = 0$, this reduces to:

$$\gamma_{11} = \text{Tr}\left[\rho\left(\hat{a}^2 + 2\hat{a}^\dagger\hat{a} + 1 + \hat{a}^{\dagger 2}\right)\right], \tag{3.1.6}$$

Substituting 3.1.1 and evaluating, we find:

$$\gamma_{11} = 1, \tag{3.1.7}$$

Following the same procedure, we obtain:

$$\gamma_{22} = 1, \quad \gamma_{21} = 0, \quad \gamma_{12} = 0 \tag{3.1.8}$$

Thus, the covariance matrix for the vacuum state is finally:

$$\gamma = \begin{pmatrix} 1 & 0 \\ 0 & 1 \end{pmatrix}. \tag{3.1.9}$$

3.1.2 Coherent State

Below are some useful properties that will help us to formulate the covariance matrix of coherent states [4].

$$D^{\dagger}(\alpha)aD(\alpha) = a + \alpha \tag{3.1.10}$$

,

$$D^{\dagger}(\alpha)a^{\dagger}D(\alpha) = a^{\dagger} + \alpha^{\dagger}, \tag{3.1.11}$$

$$D^{\dagger}(\alpha)D(\alpha) = 1 \implies D^{\dagger}(\alpha) = D^{-1}(\alpha), \tag{3.1.12}$$

$$\langle \alpha | a | \alpha \rangle = \alpha, \tag{3.1.13}$$

$$\langle \alpha | a^{\dagger} | \alpha \rangle = \alpha^{\dagger}, \tag{3.1.14}$$

$$\hat{X}\hat{X} = a^2 + 1 + 2a^{\dagger}a + a^{\dagger 2}, \tag{3.1.15}$$

$$\hat{X}\hat{P} = a^2 - a^{\dagger 2}, \tag{3.1.16}$$

$$\hat{P}\hat{X} = a^2 - a^{\dagger 2}, \tag{3.1.17}$$

$$\hat{P}\hat{P} = a^2 - 2aa^{\dagger} + 1 - a^{\dagger 2}, \tag{3.1.18}$$

The quadrature operators $\hat{X}$ and $\hat{P}$ are defined as:

19

$$\hat{X} = \frac{a + a^\dagger}{\sqrt{2}}, \tag{3.1.19}$$

$$\hat{P} = \frac{a - a^\dagger}{i\sqrt{2}}, \tag{3.1.20}$$

A 2×2 covariance matrix is given by:

$$\gamma = \begin{pmatrix} \gamma_{11} & \gamma_{12} \\ \gamma_{21} & \gamma_{22} \end{pmatrix}. \tag{3.1.21}$$

Now, calculating each element of the above matrix:

$$\gamma_{11} = \text{Tr}(|\alpha\rangle\langle\alpha|\hat{X}\hat{X}), \tag{3.1.22}$$

Now, writing our coherent state $|\alpha\rangle$ as the displaced vacuum state $D(\alpha)|0\rangle$, we get:

$$\gamma_{11} = \text{Tr}(D(\alpha)|0\rangle\langle 0|D^\dagger(\alpha)\hat{X}\hat{X}), \tag{3.1.23}$$

Now, manipulating the cyclic property of trace and using the values of $\hat{X}\hat{X}$:

$$\gamma_{11} = \text{Tr}(\langle 0|D^\dagger(a^2 + 1 + 2a^\dagger a + a^{\dagger 2})D|0\rangle), \tag{3.1.24}$$

Now, using the properties given one by one and simplifying:

$$\gamma_{11} = 1, \tag{3.1.25}$$

Similarly, we calculate the rest of the elements of our gamma matrix:

$$\gamma_{12} = \text{Tr}(|\alpha\rangle\langle\alpha|\hat{X}\hat{P}) = 0, \tag{3.1.26}$$

$$\gamma_{21} = \text{Tr}(|\alpha\rangle\langle\alpha|\hat{P}\hat{X}) = 0, \tag{3.1.27}$$

$$\gamma_{22} = \text{Tr}(|\alpha\rangle\langle\alpha|\hat{P}\hat{P}) = 1, \tag{3.1.28}$$

Plugging these values into our gamma matrix, we get:

20

$$\gamma = \begin{pmatrix} 1 & 0 \\ 0 & 1 \end{pmatrix}. \tag{3.1.29}$$

We see that the covariance matrix for the coherent state is an identity matrix.

3.1.3 Single Mode Squeezed Vacuum State

A squeezed state is given by:

$$|\alpha, \zeta\rangle = D(\alpha)S(\zeta)|0\rangle. \tag{3.1.30}$$

where $D(\alpha)$ is the displacement operator and $S(\zeta)$ is the squeezing operator. Here, ζ is the squeezing parameter and is given as $\zeta = re^{2i\phi}$.

Below are some useful properties associated with the squeezing parameter that will help us in calculating the required covariance matrix:

$$S^\dagger(\zeta)S(\zeta) = 1 \implies S^\dagger(\zeta) = S^{-1}(\zeta), \tag{3.1.31}$$

$$S^\dagger(\zeta)aS(\zeta) = a\cosh r - a^\dagger e^{2i\phi}\sinh r, \tag{3.1.32}$$

$$S^\dagger(\zeta)a^\dagger S(\zeta) = a^\dagger \cosh r - a e^{2i\phi}\sinh r, \tag{3.1.33}$$

Now, using the above-mentioned properties, we shall calculate the γ matrix of the squeezed state:

$$\gamma = \begin{pmatrix} \gamma_{11} & \gamma_{12} \\ \gamma_{21} & \gamma_{22} \end{pmatrix}. \tag{3.1.34}$$

The element γ_{11} is given by:

$$\gamma_{11} = \text{Tr}\left(|\alpha, \zeta\rangle\langle\alpha, \zeta|\hat{X}\hat{X}\right), \tag{3.1.35}$$

Using the cyclic property of trace and substituting the values of $\hat{X}\hat{X}$, we get:

21

$$\gamma_{11} = \text{Tr}\left(\langle 0|D^{\dagger}(\alpha)S^{\dagger}(\zeta)\left(\hat{a}^2 + 1 + 2\hat{a}^{\dagger}\hat{a} + \hat{a}^{\dagger 2}\right)D(\alpha)S(\zeta)|0\rangle\right), \tag{3.1.36}$$

By using the properties mentioned and solving further, we get:

$$\gamma_{11} = e^{-2r}, \tag{3.1.37}$$

Similarly,

$$\gamma_{12} = \text{Tr}\left(|\alpha,\zeta\rangle\langle\alpha,\zeta|\hat{X}\hat{P}\right) = 0, \tag{3.1.38}$$

$$\gamma_{21} = \text{Tr}\left(|\alpha,\zeta\rangle\langle\alpha,\zeta|\hat{P}\hat{X}\right) = 0, \tag{3.1.39}$$

$$\gamma_{22} = \text{Tr}\left(|\alpha,\zeta\rangle\langle\alpha,\zeta|\hat{P}\hat{P}\right) = e^{2r}, \tag{3.1.40}$$

Plugging in these values into the γ matrix, we get:

$$\gamma = \begin{pmatrix} e^{-2r} & 0 \\ 0 & e^{2r} \end{pmatrix} \tag{3.1.41}$$

3.1.4 Two mode Squeezed Vacuum State

A two-mode squeezed vacuum state (TMSVS) is represented simply as:

The simplest form of a two-mode squeezed vacuum state is given by:

$$|\psi\rangle = S(\zeta)|0,0\rangle. \tag{3.1.42}$$

Where $S(\zeta)$ is the squeezing operator defined as:

$$S(\zeta) = \exp(\zeta(a_1 a_2 - a_1^{\dagger} a_2^{\dagger})), \tag{3.1.43}$$

In the photon number basis, the squeezing operator can be expressed as:

$$S(\zeta) = \sqrt{1-\lambda}\sum_{n=0}^{\infty}\sqrt{\frac{1-\lambda}{2}}|0,0\rangle, \tag{3.1.44}$$

The density matrix of the two-mode squeezed vacuum state is given by:

$$\rho = |\psi\rangle\langle\psi| = S(\zeta)|0,0\rangle\langle 0,0|S^{\dagger}(\zeta), \tag{3.1.45}$$

The covariance matrix of the TMSVS is a 4x4 matrix denoted as:

$$\gamma = \begin{pmatrix} \gamma_{11} & \gamma_{12} & \gamma_{13} & \gamma_{14} \\ \gamma_{21} & \gamma_{22} & \gamma_{23} & \gamma_{24} \\ \gamma_{31} & \gamma_{32} & \gamma_{33} & \gamma_{34} \\ \gamma_{41} & \gamma_{42} & \gamma_{43} & \gamma_{44} \end{pmatrix}, \tag{3.1.46}$$

Where:

$$\gamma_{11} = \text{Tr}(\rho X_1 X_1), \tag{3.1.47}$$

Using the identities:

$$X_1 = \frac{a_1 + a_1^\dagger}{\sqrt{2}}, \quad X_2 = \frac{a_2 + a_2^\dagger}{\sqrt{2}}, \tag{3.1.48}$$

$$P_1 = \frac{a_1 - a_1^\dagger}{\sqrt{2}}, \quad P_2 = \frac{a_2 - a_2^\dagger}{\sqrt{2}}, \tag{3.1.49}$$

The equation for γ_{11} becomes:

$$\gamma_{11} = \frac{1}{2}\text{Tr}(\rho(a_1^2 + a_1 a_1^\dagger + a_1^\dagger a_1 + a_1^{\dagger 2})), \tag{3.1.50}$$

using the expressions from Eqn 3.1.45 we have:

$$\gamma_{11} = \frac{1}{2}\langle 0,0|S^\dagger(\zeta^*)(a_1^2 + a_1 a_1^\dagger + a_1^\dagger a_1 + (a_1^\dagger)^2)S(\zeta)|0,0\rangle. \tag{3.1.51}$$

By solving, we get:

$$\langle 0,0|S^\dagger(\zeta^*)a_1^2 S(\zeta)|0,0\rangle = \cosh r \sinh r, \tag{3.1.52}$$

$$\langle 0,0|S^\dagger(\zeta^*)(a_1^\dagger)^2 S(\zeta)|0,0\rangle = \cosh r \sinh r, \tag{3.1.53}$$

$$\langle 0,0|S^\dagger(\zeta^*)a_1 a_1^\dagger S(\zeta)|0,0\rangle = 0, \tag{3.1.54}$$

$$\langle 0,0|S^\dagger(\zeta^*)a_1^\dagger a_1 S(\zeta)|0,0\rangle = 0, \tag{3.1.55}$$

Therefore, we have:

$$\gamma_{11} = \cosh r \sinh r + \cosh r \sinh r, \tag{3.1.56}$$

$$\gamma_{11} = \sinh 2r, \tag{3.1.57}$$

Similarly solving for other entities, the final form of the covariance matrix of TMSVS is:

$$\gamma = \begin{pmatrix} \sinh(2r) & 0 & \cosh^2(r) - 1 & 0 \\ 0 & \sinh(2r) & 0 & 1 - \cosh^2(r) \\ \cosh^2(r) - 1 & 0 & \sinh(2r) & 0 \\ 0 & 1 - \cosh^2(r) & 0 & \sinh(2r) \end{pmatrix}, \tag{3.1.58}$$

The covariance matrix in terms of variance V of the quadrature operators in ket-notation is given by:

$$|\psi\rangle = \left(\frac{2}{V+1}\right)^{\frac{1}{2}} \sum_{k=0}^{\infty} \left(\frac{V-1}{V+1}\right)^{\frac{k}{2}} |k,k\rangle, \tag{3.1.59}$$

The covariance matrix of this state in terms of variance is given by:

$$\Sigma = \begin{pmatrix} V & 0 & \sqrt{V^2-1} & 0 \\ 0 & V & 0 & -\sqrt{V^2-1} \\ \sqrt{V^2-1} & 0 & V & 0 \\ 0 & -\sqrt{V^2-1} & 0 & V \end{pmatrix}, \tag{3.1.60}$$

$$\Sigma = \begin{pmatrix} V\mathbb{1} & \sqrt{V^2-1}\,\sigma_z \\ \sqrt{V^2-1}\,\sigma_z & V\mathbb{1} \end{pmatrix}. \tag{3.1.61}$$

Where $\sigma_z = \begin{pmatrix} 1 & 0 \\ 0 & -1 \end{pmatrix}$.

3.2 Gaussian Quantum Operations

Symplectic operators are Gaussian unitary operators or functions that obey the following property:

$$S\Omega S^\dagger = \Omega \tag{3.2.1}$$

24

Here, S denotes a symplectic matrix or operator [15]. In a Hilbert space, unitary transformations are those that are symplectic, such that:

$$x \to Sx \tag{3.2.2}$$

$$\Sigma = S\Sigma S^T, \tag{3.2.3}$$

The most important symplectic operator used in this context is the beam splitter. Its matrix form, in terms of the channel transmission T, is given by:

$$\mathrm{BS} = \begin{pmatrix} \sqrt{T}\mathbb{1} & \sqrt{T^2-1}\mathbb{1} \\ \sqrt{T^2-1}\mathbb{1} & -\sqrt{T}\mathbb{1} \end{pmatrix}, \tag{3.2.4}$$

Thus far, we have formulated important channels that can be utilized in a quantum communication setup. In the next chapter, we develop a setup based on above resources

3.3 Transmittance and Noise

In the Alice-Bob communication channel, the overall noise can be represented as the summation of various contributing factors:

$$E = \frac{1-T}{T} + \frac{E_{\det}}{T} + \varepsilon_A, \tag{3.3.1}$$

The first term, $\frac{1-T}{T}$, denotes the loss generated in the vacuum condition, often referred to as channel losses. The second term, $\frac{E_{\det}}{T}$, represents the imperfections of the homodyne detection process. The third term, ε_A, accounts for excess noise originating from Alice's input rather than from detector imperfections or channel losses.

The noise due to the homodyne detector can be expressed as:

$$E_{\det} = \frac{1+v_{\mathrm{el}}}{\eta} - 1, \tag{3.3.2}$$

Alternatively:

$$E_{\det} = \frac{1-\eta_{\det}}{\eta_{\det}} + \frac{v_{\mathrm{el}}}{\eta_{\det}}, \tag{3.3.3}$$

Where:

- η is the detection efficiency.

- v_{el} is the electronic noise of the detector.

The total quadrature variance V_B measured by Bob can be given by:

$$V_B = T_{\mathrm{ch}}\eta_{\mathrm{det}}(V + E), \tag{3.3.4}$$

This can be further expanded to:

$$V_B = T_{\mathrm{ch}}\eta_{\mathrm{det}}\left(V + \frac{1 - T_{\mathrm{ch}}}{T_{\mathrm{ch}}} + \zeta_A + \frac{1 - \eta_{\mathrm{det}}}{T_{\mathrm{ch}}\eta_{\mathrm{det}}} + \frac{v_{\mathrm{el}}}{T_{\mathrm{ch}}\eta_{\mathrm{det}}}\right), \tag{3.3.5}$$

Simplifying this, we get:

$$V_B = T(V - 1) + 1 + T\zeta_A + v_{\mathrm{el}}, \tag{3.3.6}$$

Assuming $v_{\mathrm{el}} = \zeta_{\mathrm{det}}$ (as we treat it as an excess noise), the equation becomes:

$$T\zeta_A + v_{\mathrm{el}} = T\zeta_A + \zeta_{\mathrm{det}} = T\left(\zeta_A + \frac{\zeta_{\mathrm{det}}}{T}\right) = T\zeta_{\mathrm{tot},A}, \tag{3.3.7}$$

Given that the excess noise is defined with respect to the measurement location, we have:

$$\zeta = \zeta_{\mathrm{tot},B} = \zeta_{\mathrm{tot},A}, \tag{3.3.8}$$

Thus, V_B simplifies to:

$$V_B = T(V - 1) + 1 + \zeta, \tag{3.3.9}$$

$$V_B = TV_{\mathrm{mod}} + 1 + \zeta, \tag{3.3.10}$$

In practical systems, the transmission T is defined as:

$$T = T_{\mathrm{ch}}\eta_{\mathrm{coup}}\eta_{\mathrm{det}}, \tag{3.3.11}$$

And the total excess noise ζ includes various noise sources such as:

$$\zeta = \zeta_{\text{mod}} + \zeta_{\text{Raman}} + \zeta_{\text{quant}} + \zeta_{\text{phase}} + \zeta_{\text{det}} + \zeta_{\text{RIN}} + \dots, \tag{3.3.12}$$

The overall noise in the Alice-Bob channel is a combination of channel losses, detection imperfections, and excess noise from various sources. The variance measured by Bob includes contributions from the channel, detection efficiency, and various noise factors. The effective transmission factor and the cumulative noise from multiple sources define the actual performance of the communication channel.

Generalized approach to Gaussian Network

4.1 Gaussian Quantum states

The process of creating continuous variables in many optical setups have revealed the complex process of multimode-entangled states. It is through reconfigurable Gaussian interactions, imprinted cluster states, and entanglement correlations that these states naturally arise [16, 22]. The quadrature $\hat{q}_j$ and $\hat{p}_j$ are canonical conjugate variables for the j-th optical mode, comparable to position and momentum in quantum mechanics. They satisfy the commutation relation,

$$[\hat{q}_j, \hat{p}_k] = i\delta_{j,k}. \tag{4.1.1}$$

This fundamental relation ensures that $\hat{q}_j$ and $\hat{p}_j$ are indivisibly linked, reflecting the Heisenberg uncertainty principle. '$\hat{a}^\dagger$'and '$\hat{a}$' are the operators related to quadrature.

The quadratures relate to the creation $\hat{a}^\dagger$ and annihilation $\hat{a}$ operators of the quantum harmonic oscillator, which describes the light mode [27]. The relations are given by:

$$\hat{a}^\dagger = \frac{1}{\sqrt{2}}(\hat{q} - i\hat{p}), \tag{4.1.2}$$

$$\hat{a} = \frac{1}{\sqrt{2}}(\hat{q} + i\hat{p}). \tag{4.1.3}$$

Here, the vacuum quadratures variance is normalized to $\frac{1}{2}$. The first two moments of the quadrature can fully describe the Gaussian states:

$$\bar{r} = \mathrm{Tr}[\rho \hat{r}], \tag{4.1.4}$$

This is the quadrature vector's mean value, $\hat{r}$, where ρ is the Gaussian state's density matrix. The covariance matrix of the quadratures

$$\sigma = \text{Tr}[\rho\{(\hat{r} - \bar{r}), (\hat{r} - \bar{r})^T\}], \tag{4.1.5}$$

provides information on the spread and correlations between them. Quadratic Hamiltonian characterizes parametric processes :

$$\hat{H}_I = \hat{r} H \hat{r}^T, \tag{4.1.6}$$

This Hamiltonian describes the interaction and evolution of the system in terms of the quadrature vector $\hat{r}$.

The dynamics of the quadratures are governed by the symplectic transformation

$$S_H = e^{\Omega H t}, \tag{4.1.7}$$

where Ω is the symplectic matrix and H is the Hamiltonian matrix.

The initial quadratures $\hat{r}_0$ evolve to the final quadratures $\hat{r}'$ as:

$$\hat{r}' = S_H \hat{r}_0, \tag{4.1.8}$$

The matrix Ω is part of the symplectic structure that preserves the commutation relations during the system's evolution. The exact form of Ω is crucial in defining how the quadratures transform under the Hamiltonian dynamics. The commutation relation is given by:

$$[\hat{r}, \hat{r}^T] = i\Omega = i \begin{pmatrix} 0 & 1 \\ -1 & 0 \end{pmatrix}. \tag{4.1.9}$$

By applying a unitary operation produced by a quadratic Hamiltonian H to the vacuum state, one can obtain any pure Gaussian state [27]. Thus, the vacuum covariance matrix $\sigma_0 = \frac{1}{2}$ can be transformed into the most generic version of the covariance matrix for a pure Gaussian state by using the symplectic transformation S_H. This leads to:

$$\sigma = S_H \sigma_0 S_H^T = \frac{1}{2} S_H S_H^T, \tag{4.1.10}$$

The Bloch-Messiah decomposition can be used to express the symplectic transformation as a product of orthogonal and diagonal matrices using singular value decomposition: $S_H = O\Delta O_0$. Substitute $S_H = O\Delta O_0$ into the equation:

$$\sigma = \frac{1}{2}(O\Delta O_0)(O\Delta O_0)^T, \tag{4.1.11}$$

Note that for any matrices A, B, and C:

$$(ABC)^T = C^T B^T A^T, \tag{4.1.12}$$

Therefore:

$$(O\Delta O_0)^T = O_0^T \Delta^T O^T, \tag{4.1.13}$$

Since Δ is a diagonal matrix, $\Delta^T = \Delta$, so:

$$(O\Delta O_0)^T = O_0^T \Delta O^T, \tag{4.1.14}$$

Combine the expressions:

$$\sigma = \frac{1}{2}(O\Delta O_0)(O_0^T \Delta O^T), \tag{4.1.15}$$

Since O_0 is an orthogonal matrix, $O_0^T O_0 = I$:

$$\sigma = \frac{1}{2}O\Delta(O_0 O_0^T)\Delta O^T, \tag{4.1.16}$$

therefore:

$$\sigma = \frac{1}{2}O\Delta I \Delta O^T = \frac{1}{2}O\Delta^2 O^T. \tag{4.1.17}$$

We can understand this as a rotation of basis, followed by a squeezing in the diagonal basis, and finally a rotation. The basis in which the covariance matrix is diagonal and the different components are independently squeezed is called the supermode basis. The squeezing parameters in (Δ) come from the eigenvalues of the Hamiltonian $\hat{H}_I$, while the orthogonal matrix O is a passive linear optical transformation or an active change of measurement basis. We do not care about the orthogonal matrix O_0 anymore in the product $S_H S_H^T$, thus it can be safely ignored, hence:

$$\sigma = \frac{1}{2} S_H S_H^T = \frac{1}{2} O \Delta^2 O^T \tag{4.1.18}$$

In the case of a single-mode field, the squeezing operation, a Gaussian transformation, decreases the variance of $\hat{p}$ by a factor of $10^{-s/10}$, where s in dB is the squeezing factor. The squeezing operation is given using this local symplectic matrix:

$$S_{\text{sq}}(s) = \begin{pmatrix} 10^{s/20} & 0 \\ 0 & 10^{-s/20} \end{pmatrix} \tag{4.1.19}$$

For multiple modes, the Δ matrix is expressed as:

$$\Delta = \text{diag}\left(10^{s_1/20}, 10^{s_2/20}, \ldots, 10^{s_N/20}, 10^{-s_1/20}, 10^{-s_2/20}, \ldots, 10^{-s_N/20}\right) \tag{4.1.20}$$

This framework can be exploited for the visualization and manipulation of Gaussian quantum states which are easily accessible in state-of-the-art photonics laboratories. Whereas, at this stage, the number of modes and their interconnections are limited, intensive efforts are underway to extend these systems.

4.2 Gaussian Networks

A Gaussian network is such a quantum network in which quantum states of nodes or modes are Gaussian states, and operations among these are Gaussian operations. The Gaussian states, including coherent states and squeezed states, are represented as Gaussian functions in the phase space and are completely defined by their mean vector and covariance matrix. In quantum networks, let's explore various topologies (linear, ring, star, wheel, fully connected, and grid). When considering these topologies in the context of Gaussian networks, the nodes represent Gaussian states, and the edges represent Gaussian operations. The squeezing cost, which is a measure of the resources needed to maintain entanglement or quantum correlations across the network, plays a critical role.

4.2.1 Linear Graph

In a linear topology, nodes are arranged in a straight line, with each node connected to its immediate neighbor, resulting in n vertices and $n-1$ connections. This simple structure is characterized by sequential connectivity, making it straightforward to analyze and implement.
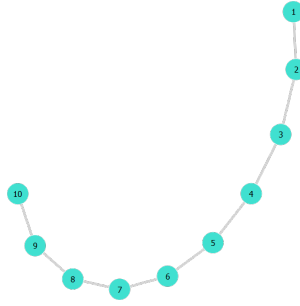
Figure 4.1: Linear Graph

4.2.2 Cycle Graph

The cycle topology extends the linear topology by connecting the last node back to the first, forming a closed loop. It consists of n nodes and n connections, with each node connected to exactly two adjacent nodes, creating a circular structure that enhances redundancy.
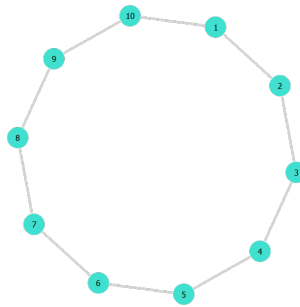

Figure 4.2: Cycle Graph

4.2.3 Wheel Graph

The wheel topology is a combination of the star and ring topologies. It includes N nodes, with one central node connected to all peripheral nodes, and the peripheral nodes forming a ring. This results in $2n - 1$ edges, providing both centralized and distributed connectivity.
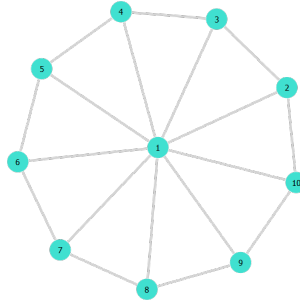
Figure 4.3: Wheel Graph

4.2.4 Star Graph

In a star topology, a single central node is directly connected to every other node in the network, whereas the peripheral nodes do not interconnect. This topology has N nodes (1 central node and $N-1$ peripheral nodes) and $N-1$ edges, making the central node a critical hub for communication.
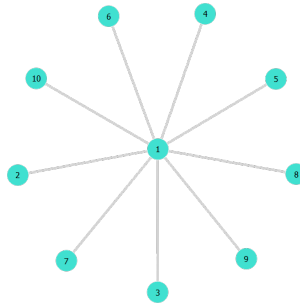
Figure 4.4: Star Graph

4.2.5 Complete Graph

A fully connected topology is the most interconnected structure, where every node is directly connected to every other node. With N nodes and $\frac{n(n-1)}{2}$ edges, this topology ensures maximum connectivity, though it can be complex and resource-intensive.

4.2.6 Grid Graph

In a grid topology, nodes are arranged in a grid pattern, such as a $m \times n$ grid, where each node is typically connected to its four adjacent neighbors (except for edge and corner nodes). This

Figure 4.5: Compelete Graph

structure consists of nodes and $2mn - m - n$ edges, creating a regular, structured network ideal for certain types of applications.
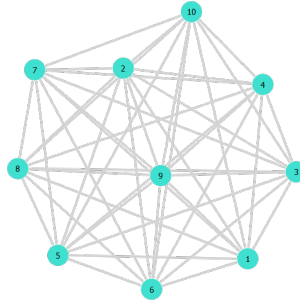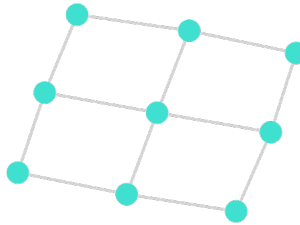

Figure 4.6: Grid Graph

4.3 Exploring the Graph states in Quantum Networks

A graph $G(V,E)$ can be used to mathematically indicate a network, where V is the number of vertices or nodes, and E is the set of edges connecting these vertices. A symmetric adjacency matrix $A = A^T$ naturally results if we label the nodes in a particular order. This matrix's entry A_{jk} at position (j,k) indicates the weight of the edge that connects node j to node k; if there is no such edge, the weight is zero.

For most purposes, an adjacency matrix is all there is to be said about a graph, but for our application, node squeezing and angle are relevant parameters too. We now discuss the quantum networks adopted here: graph states or cluster states. These networks can be prepared by entangling multiple squeezed light modes via Controlled-Z gates. A Gaussian operation known as a controlled-Z gate correlates the $\hat{q}$ and $\hat{p}$ quadratures of the modes it works upon with strength g. In symplectic operations, the matrix is

$$S_{CZ}(g) = \begin{pmatrix} 1 & 0 & 0 & 0 \\ 0 & 1 & 0 & 0 \\ 0 & g & 1 & 0 \\ g & 0 & 0 & 1 \end{pmatrix}. \qquad (4.3.1)$$

The edges in the graph corresponding to a graph state [8, 12, 29] correspond to squeezed modes or CZ-gates applied between nodes, and their weight is determined by the parameter g. Assuming that all nodes are compressed in the $\hat{p}$ quadrature by a factor s and that all edges have a correlation strength g, we will now simplify the various degrees of freedom in our networks.

A vacuum state that is compressed into several modes, denoted as σ_s, is categorized by its squeezing factor s. The degree of noise reduction in one quadrature, $\hat{p}$ for example, at the expense of increased noise in the conjugate one, $\hat{q}$, is determined by the squeezing factor s.

The variance matrix σ_s of a squeezed vacuum state is generally diagonal and reads:

$$\sigma_s = \begin{pmatrix} RI_N & 0 \\ 0 & R^{-1}I_N \end{pmatrix}, \qquad (4.3.2)$$

where $R = 10^{s/10}$ and I_N is the $N \times N$ identity matrix. The symplectic matrix S for the CZ-gate network is:

$$S = \begin{pmatrix} 1 & 0 \\ A & 1 \end{pmatrix}, \qquad (4.3.3)$$

Applying the transformation:

$$\sigma = S\sigma_s S^T = \begin{pmatrix} 1 & 0 \\ A & 1 \end{pmatrix} \begin{pmatrix} RI_N & 0 \\ 0 & R^{-1}I_N \end{pmatrix} \begin{pmatrix} 1 & A^T \\ 0 & 1 \end{pmatrix}, \qquad (4.3.4)$$

When an adjacency matrix A describing a CZ-gate network is applied to a multimode squeezed vacuum state σ_s with squeezing factor s, it gives a Gaussian network whose covariance matrix σ [32] is defined as:

$$\sigma = \begin{pmatrix} \sigma_{qq} & \sigma_{qp} \\ \sigma_{pq} & \sigma_{pp} \end{pmatrix} = \begin{pmatrix} R & RA^T \\ RA & RA^2 + R^{-1} \end{pmatrix}, \qquad (4.3.5)$$

The blocks σ_{qq} and σ_{pp} represent the intraquadrature correlations of q and p of different nodes,

respectively. The blocks σ_{qp} and σ_{pq}, on the other hand, represent the inter-quadrature correlations between q and p.

Note that the theoretical CZ-gate operations, which define network edges, are seldom practically implemented due to their complexity. Generally, a method of building the graph state from several squeezed modes and linear optical transformations is shown along with a simplification of the graph state's covariance matrix.

It can be demonstrated that an initial uniform squeezing adds only a constant factor to the end squeezing cost, thus we take a vacuum state in an initial set of N modes that are un-squeezed, $s = 0$. Also, assuming that the adjacency matrix A is symmetric $A = A^T$, and the coupling strength for each edge of the graph g is 1, the final covariance matrix for N-modes is:

$$\sigma = \frac{1}{2} \begin{pmatrix} \mathbb{1} & A \\ A & \mathbb{1} + A^2 \end{pmatrix}. \tag{4.3.6}$$

where the vacuum state normalized variance equal to 1/2.

4.4 Quantifying Squeezing: A Resource Theory Perspective

The fundamental building blocks of continuous variable quantum information are Gaussian bosonic states, which have significant uses in quantum optics. These states serve as essential building blocks for numerous cutting-edge quantum technologies, such as multi-party quantum communication, measurement-based quantum computation, quantum simulations [26], and quantum metrology [13, 24]. In the discussion of the correlations between Gaussian states, the first moments (mean values) are less important. Although first moments are relevant for any realistic quantum computation or communication protocol, their computation is usually done in classical post-processing, and they do not enter the evolution of the second moments. Thus, we can focus on the covariance matrix to fully describe these quantum states. The covariance matrix is a key descriptor of Gaussian states. It captures the quadrature operators' second moments (variances and covariances). Squeezing is essential for creating Gaussian entangled states. The resource theory aims to provide a systematic way to quantify the resources required for creating and manipulating Gaussian states, which are essential for various quantum information protocols. Resources typically refer to specific properties or quantities that are necessary for performing quantum tasks. For Gaussian states, squeezing is a primary resource [28]. These are linear transformations that preserve the symplectic structure of phase space.They are essential

to the modulation of Gaussian states and provide a quantitative indicator of how much squeezing is occurring within a state. This measure is essential because squeezing directly impacts the state's utility in quantum information tasks. The "squeezing cost" refers to a measure of the resources required to produce a quantum state with a certain amount of squeezing. In [21], a specific approach to measuring squeezing is discussed, where an operational squeezing measure for any symplectic transformation T is defined by:

$$M : \mathbb{R}^{2N \times 2N} \to \mathbb{R}, \quad M(T) = 20 \sum_{j=1}^{N} \log_{10} \sqrt{\mu_j^+(T)}, \tag{4.4.1}$$

Here, $\mu_j^+(T)$ denotes the largest singular values of T, and the factor of 20 ensures the result is in decibels (dB). From Eqn. 4.4.1, a squeezing measure for covariance matrices can be defined as:

$$S : \mathbb{R}^{2N \times 2N} \to \mathbb{R}, \quad S(\sigma) = \sum_{j=1}^{N} 10 \log_{10} \mu_j^+(2\sigma). \tag{4.4.2}$$

where $\mu_j^+(2\sigma)$ represents the largest singular values of 2σ. Multiplying the covariance matrix by 2 ensures that the vacuum state has zero cost. The latter definition can be generalized to arbitrary quantum states but is most simple for pure Gaussian states and applies, in general, to any number of modes.

4.5 Network Generation via Squeezing cost

4.5.1 squeezing cost vs Node

The Covariance matrix σ for the general Network which we discussed with detail in Sec 4.3 is given as:

$$\sigma = \frac{1}{2} \begin{pmatrix} \mathbb{1} & A \\ A & \mathbb{1} + A^2 \end{pmatrix}, \tag{4.5.1}$$

where A is the Adjacency matrix with $(A_i, A_j) = 0$ for non-adjacent nodes and $(A_i, A_j) = 1$ for adjacent nodes. Measuring the largest singular values of the covariance matrix σ and substituting these values in the Eqn 4.4.2 to find the squeezing cost of a given network.

4.5.2 Squeezing cost vs Mode

We want to analyze each mode independently, so we make some transformations in the Covariance matrix σ to treat each mode separately. Since A is symmetric, it is always diagonalizable. We can find an orthogonal matrix U such that:

$$UAU^T = \Lambda = \text{diag}(\lambda_i), \tag{4.5.2}$$

where λ_i are the real eigenvalues of A. Consequently, we have $UA^2U^T = (UAU^T)^2 = \Lambda^2$. Consider the orthogonal matrix P defined as:

$$P = \frac{1}{\sqrt{2}} \begin{pmatrix} U & U \\ U & -U \end{pmatrix}, \tag{4.5.3}$$

It is easy to verify that $PP^T = I$, confirming that P is indeed orthogonal.

Applying P to Σ, we get:

$$\sigma' = P\sigma P^T = \frac{1}{2} \begin{pmatrix} I + \Lambda + \Lambda^2/2 & -\Lambda^2/2 \\ -\Lambda^2/2 & I - \Lambda + \Lambda^2/2 \end{pmatrix}, \tag{4.5.4}$$

Here, σ' is a block matrix of the form where the entries are diagonal matrices. Using this, we can perform a permutation on the rows and columns of σ' yielding:

$$Q = \bigoplus_{i=1}^{N} N_i, \tag{4.5.5}$$

Each block N_i is given by:

$$N_i = \frac{1}{2} \begin{pmatrix} 1 + \lambda_i + \lambda_i^2/2 & -\lambda_i^2/2 \\ -\lambda_i^2/2 & 1 - \lambda_i + \lambda_i^2/2 \end{pmatrix}. \tag{4.5.6}$$

That is, each block N_i represents a single-mode covariance matrix of some pure, unentangled Gaussian state.. Each block N_i can be independently diagonalized. Notably, the determinant of N_i is:

$$\det(N_i) = \frac{1}{4}, \tag{4.5.7}$$

The eigenvalues of N_i are:

$$\eta_i = \frac{1}{2}\left(1 + \frac{\lambda_i^2}{2} \pm \sqrt{\left(1 + \frac{\lambda_i^2}{2}\right)^2 - 1}\right). \tag{4.5.8}$$

These eigenvalues represent the squeezed and anti-squeezed quadratures of the Gaussian states. The block diagonal form reveals the individual covariance matrices N_i for each mode. These matrices contain information about the squeezing parameters of the Gaussian states. The block diagonal form indicates that the states are unentangled in the new basis. This is crucial for understanding the individual properties of each mode without interference from other modes. After calculating the eigenvalues of each block substitute them in the Eqn 4.4.2 to get the squeezing cost against each mode.

4.6 Modeling Gaussian Quantum Channel

We need to model the channel through which our states travel, ensuring that the channel maintains the Gaussian nature of our states. Two Gaussian channels are pure-loss/bosonic-loss channels and thermal loss channels. Pure-loss channels are simpler to model as they do not consider thermal noise. By adding a beam splitter loss to the signal data, they can be modeled. This is done by mixing the incoming signal with a vacuum input, delineating our model for bosonic loss states (Figure 2.6). Let us implement this model on N mode Gaussian graph state

$$\sigma' = \hat{B}(\tau_c)\hat{\sigma}\hat{B}^T(\tau_c). \tag{4.6.1}$$

The beam splitter transformation for a pure-loss channel is represented by the matrix $\hat{B}(\tau_c)$. For an N-mode system, this matrix can be written as:

$$\hat{B}(\tau_c) = \begin{pmatrix} I & 0 & 0 \\ 0 & \sqrt{\tau_c}I & \sqrt{1-\tau_c}I \\ 0 & -\sqrt{1-\tau_c}I & \sqrt{\tau_c}I \end{pmatrix}, \tag{4.6.2}$$

where τ_c is the transmission coefficient (representing the fraction of the signal that is transmitted), I is the $N \times N$ identity matrix, and 0 is the $N \times N$ zero matrix. Its transpose is given as

$$\hat{B}^T(\tau_c) = \begin{pmatrix} I & 0 & 0 \\ 0 & \sqrt{\tau_c}I & -\sqrt{1-\tau_c}I \\ 0 & \sqrt{1-\tau_c}I & \sqrt{\tau_c}I \end{pmatrix}, \tag{4.6.3}$$

4.6.1 Squeezing in Pure Loss Channels vs. Nodes

The covariance matrix σ of this Gaussian graph state [31] was given by:

$$\sigma = \frac{1}{2} \begin{pmatrix} \mathbb{1} & A \\ A & \mathbb{1}+A^2 \end{pmatrix}, \tag{4.6.4}$$

After mixing input signals with a vacuum input, the transformed covariance matrix is given as

$$\sigma = \frac{1}{2} \begin{pmatrix} \mathbb{1} & A & 0 \\ A & \mathbb{1}+A^2 & 0 \\ 0 & 0 & \mathbb{1} \end{pmatrix}, \tag{4.6.5}$$

Now applying the Eqn 4.6.1 we get

$$\sigma' = \frac{1}{2} \begin{pmatrix} I & \sqrt{\tau_c}A & \sqrt{1-\tau_c}A \\ \sqrt{\tau_c}A & \tau_c(I+A^2)+(1-\tau_c)I & \sqrt{\tau_c(1-\tau_c)}(A^2-I) \\ \sqrt{1-\tau_c}A & \sqrt{\tau_c(1-\tau_c)}(A^2-1) & (1-\tau_c)(I+A^2)+(\tau_c)I \end{pmatrix}. \tag{4.6.6}$$

4.6.2 Squeezing in Pure Loss Channels vs. Modes

The covariance matrix for each mode N_i is expressed as:

$$N_i = \frac{1}{2} \begin{pmatrix} 1+\lambda_i+\frac{\lambda_i^2}{2} & -\frac{\lambda_i^2}{2} \\ -\frac{\lambda_i^2}{2} & 1-\lambda_i+\frac{\lambda_i^2}{2} \end{pmatrix}, \tag{4.6.7}$$

In this basis, each block N_i corresponds to a single-mode covariance matrix of a pure, unentangled Gaussian state, where $\{\lambda_i\}_{i=1}^N$ is the set of real eigenvalues of A.

After combining the input signals with a vacuum input, the updated N_i [31] is given by:

$$N_i = \frac{1}{2} \begin{pmatrix} 1+\lambda_i+\frac{\lambda_i^2}{2} & -\frac{\lambda_i^2}{2} & 0 \\ -\frac{\lambda_i^2}{2} & 1-\lambda_i+\frac{\lambda_i^2}{2} & 0 \\ 0 & 0 & 1 \end{pmatrix}. \tag{4.6.8}$$

then applying the Eqn 4.6.1 we get the loss in squeezing cost.

Results and Discussion

5.1 Squeezing cost of different networks

In quantum networks, the squeezing cost is a critical metric that quantifies the amount of quantum resource (squeezed light) required to maintain entanglement or quantum correlations across the network. The squeezing cost can be analyzed by examining its distribution across different modes and nodes within the network.

Modes refer to the distinct quantum states or channels through which information is transmitted in the network. Each mode represents a potential pathway for quantum correlations to be established and maintained between nodes.

Nodes represent the points or vertices in the network, typically corresponding to physical locations where quantum states are prepared, manipulated, or measured.

When analyzing the squeezing cost:

5.1.1 Squeezing cost of Nodes

When we shift our focus to nodes, the x-axis now represents the different nodes in the network. Each point along the x-axis corresponds to a specific node, allowing us to analyze the squeezing cost required to maintain quantum correlations at that particular node. As we move from one node to another, the graph shows how the resource requirements change across the network.

The y-axis remains the squeezing cost, but now it reflects the quantum resources required at each node. A higher position on the y-axis indicates that a particular node demands more squeezing to maintain the necessary quantum correlations. This part of the analysis helps to identify nodes

that might be more resource-intensive due to their connectivity or role in the network.

Cycle

Every node in a cycle graph is connected to exactly two other nodes, creating a complete loop as a sort of network structure. This indicates that each node is a link in a circular chain, with N nodes being equal to the number of edges, or connections, in the chain. The squeezing cost of a network grows linearly with the number of nodes in the network. For a cycle graph, the squeezing cost rises with the number of nodes since additional connections (edges) require the maintenance of quantum resources. As the cycle grows, more squeezing is required to preserve quantum entanglement and coherence across the entire network, making the network more resource-intensive as it scales up. This increase reflects the need for more quantum resources to manage the larger, more complex structure of the ring graph.
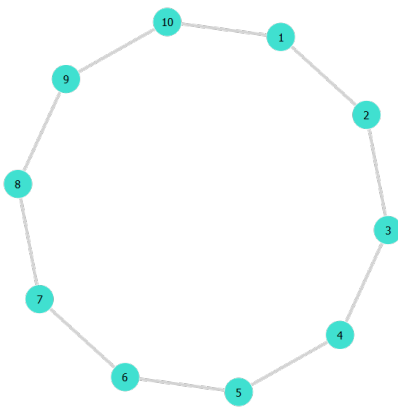
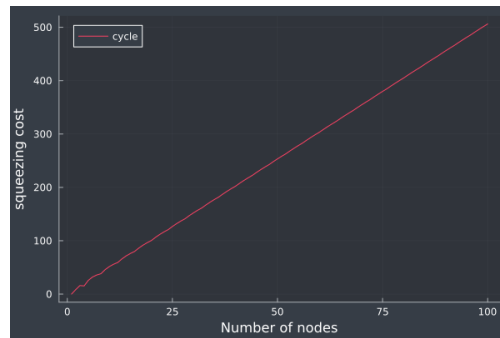**Figure 5.1:** Cycle graph with 10 nodes and 10 edges

Figure 5.2: Graph plot for cycle graph with 100 nodes in the horizontal direction and squeezing cost in the vertical direction.

Grid

In a square grid, nodes are arranged in a 2D square lattice. For example, a 4×4 grid has 16 nodes, and each node (except those on the edges) is connected to four neighbors. A square grid with N nodes (where $N = m \times m$) would have $2m(m-1)$ edges. In a square grid topology, the squeezing cost starts low due to the short paths and minimal noise accumulation in small grids. However, as the number of nodes increases, the squeezing cost grows rapidly due to the longer paths.
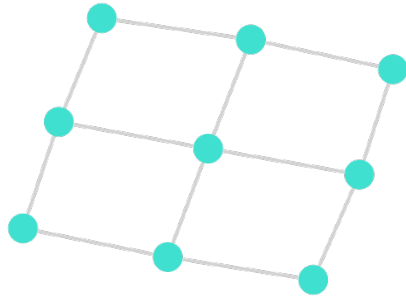
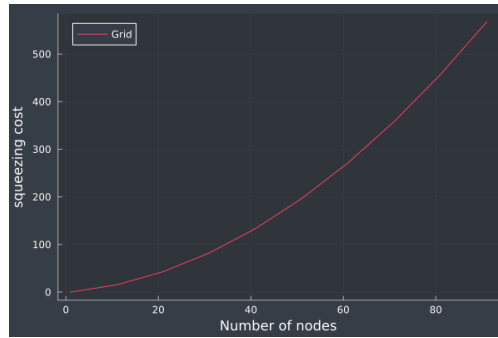**Figure 5.3:** A square 3×3 grid with 12 nodes and 9 edges

Figure 5.4: Graph plot for grid graph for 100 Nodes against squeezing cost

Linear Graph

In a linear graph, the nodes are arranged in a straight line. Each node (except for the two endpoints) is connected to exactly two neighboring nodes. The endpoints are connected to only one other node. For N nodes in a linear graph, there are $N - 1$ edges, where each edge represents a direct connection between two neighboring nodes. In a linear graph, each additional node introduces one more edge that needs squeezing. Therefore, the squeezing cost increases proportionally with the number of nodes N. This linear growth occurs because there's a direct relationship between the number of nodes and the number of edges as each new node adds exactly one new edge that needs squeezing.
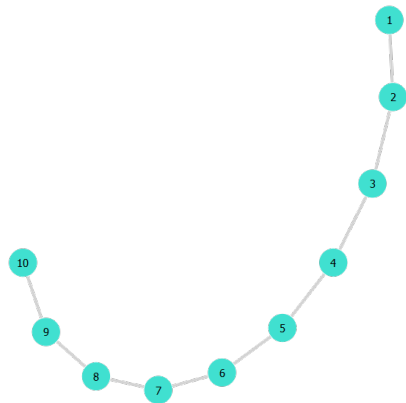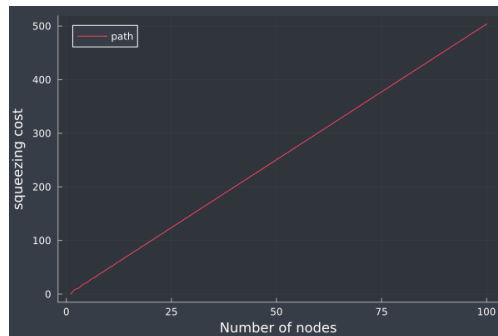

Figure 5.6: Graph plot of linear graph of squeezing cost vs 100 nodes, nodes on the x-direction and squeezing cost on the y-direction

Figure 5.5: Linear graph with 10 nodes and 9 edges

43

Star

In a star graph, there is a central hub node that is connected to all other peripheral nodes, which do not connect to each other. If there are N nodes in the star graph, there are $N-1$ edges, with each edge connecting one of the peripheral nodes to the central hub. In a star graph, all quantum resources are concentrated at the central hub, which manages all the entanglement and communication with the peripheral nodes. Because the peripheral nodes are only directly connected to the central hub, adding more nodes does not require maintaining additional direct connections between the peripheral nodes themselves. This centralized structure makes the squeezing cost increase more slowly than in a cycle graph, where every node must maintain connections with two neighbors.
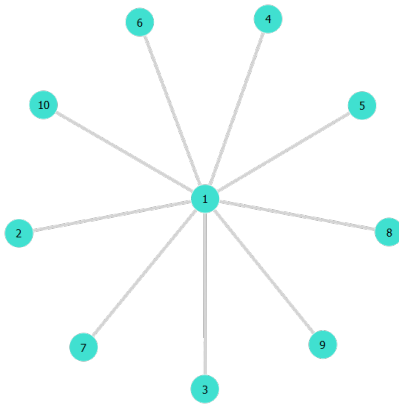

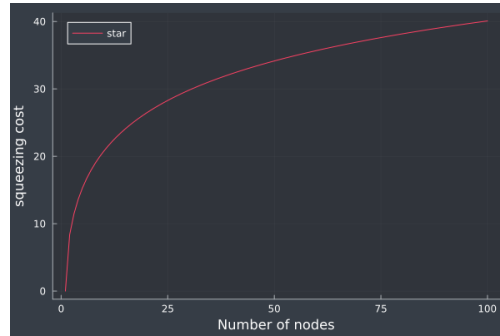**Figure 5.7:** Star graph with 10 nodes and 9 edges.

Figure 5.8: Graph plot for squeezing cost against 100 nodes for star graph

Wheel

A wheel graph is a combination of a ring graph and a star graph. It consists of a central hub node that is connected to all other nodes, and those peripheral nodes are also connected in a ring. For N nodes, the wheel graph has $N-1$ peripheral nodes forming the ring, and one central hub connected to all $N-1$ peripheral nodes. The squeezing cost for a wheel graph grows similarly to that of a ring graph because the wheel graph includes both a ring structure and a central hub. The ring structure, which requires maintaining connections among all peripheral nodes, dominates the squeezing cost, leading to a growth pattern similar to a ring graph. Although the wheel graph has a central hub like a star graph, the additional complexity of maintaining the ring connections causes the squeezing cost to increase more rapidly, aligning it more closely

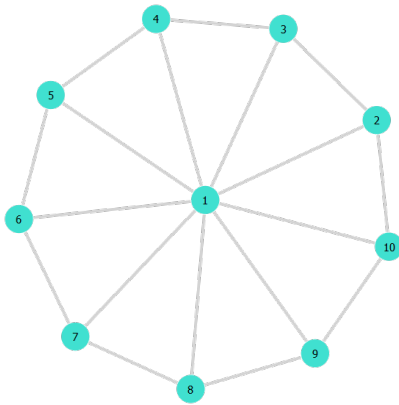with the behavior of a ring graph rather than a star graph.

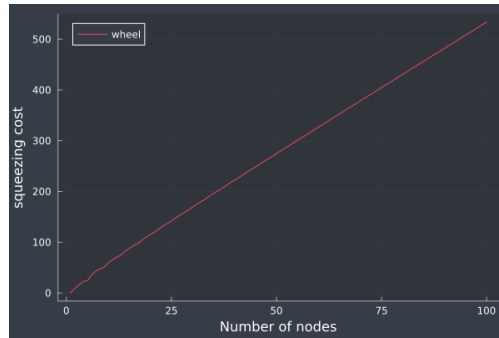**Figure 5.9:** Wheel graph with 10 nodes and 18 edges.

Figure 5.10: Graph plot for squeezing cost against 100 nodes for wheel graph

Complete Graph

In a fully connected graph, every node is connected to every other node. This results in a very dense network with a large number of edges $\frac{N(N-1)}{2}$. The squeezing cost for the fully connected graph grows linearly with the number of nodes N. This means that as we add more nodes to the network, the squeezing cost increases directly to the number of nodes.
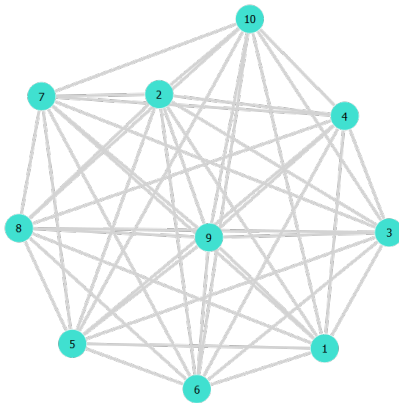

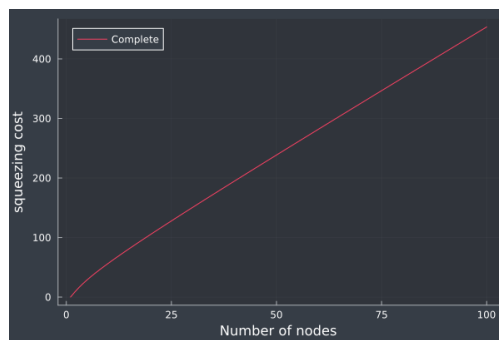**Figure 5.11:** Complete Graph with 10 nodes.

Figure 5.12: Graph plot for squeezing cost against 100 nodes for complete graph

All topoligies

The complete graph is most efficient for large networks due to the balanced distribution of squeezing resources but grows linearly with N. It offers redundancy and multiple pathways, minimizing individual node squeezing costs.

The cycle graph has linear growth in squeezing cost but with fewer edges than the complete graph, making it less resource-intensive but still requiring significant squeezing as N increases.

The star graph provides the most efficient squeezing cost for small to moderate networks due to its centralized structure. However, it becomes less efficient as the central hub becomes overloaded with more nodes.

The grid topology starts with low squeezing cost but experiences rapid growth as the network expands due to the complexity of managing correlations in a 2D lattice.

The wheel graph balances between a cycle and a central hub. It is more efficient than a grid but still experiences rapid cost increases as the number of nodes grows.

The path graph has a simple structure with linear growth in squeezing cost. It is less efficient due to the lack of redundancy and longer paths.

In summary, the squeezing cost depends on the network's connectivity, dimensionality, and the distribution of resources. Topologies like the complete graph are more efficient for large networks due to their redundancy, while star graphs offer efficiency for smaller networks. Grids and wheels, while providing good connectivity, can experience rapid increases in squeezing cost as they scale.
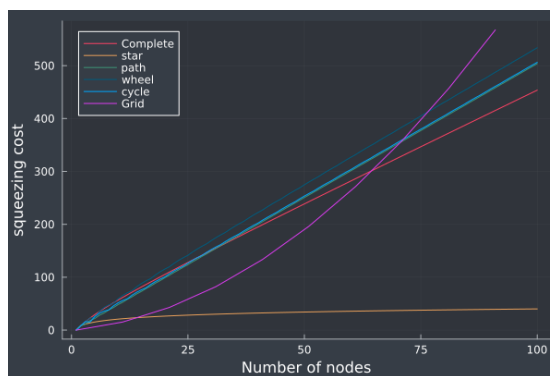

Figure 5.13: Trend of squeezing cost vs 100 nodes of different networks in which red, yellow, green, bold green, blue and purple represent the complete graph, star, path, wheel, cycle, and grid respectively.

5.1.2   Squeezing cost of Modes

The squeezing spectrum of different regular network structures particularly focuses on how the spectrum varies across various topologies when the number of N is fixed at 100. The "full squeezing spectrum" refers to the range of squeezing values (eigenvalues) associated with the modes of a network. These values are determined from the adjacency matrix of the network's graph, which encodes the connections between nodes. The x-axis of the graph represents the different modes in the network. Each mode corresponds to a specific quantum channel or state that is being analyzed. As we move along the x-axis, we consider the squeezing cost associated with each mode.

The y-axis shows the squeezing cost associated with each mode. Higher values on the y-axis indicate that a particular mode requires more quantum resources to maintain the desired level of entanglement or correlation.

Complete Graph

The presence of a single large eigenvalue in the squeezing spectrum indicates that one mode dominates the squeezing resources in the system. The other $N - 1$ modes, associated with the smaller, equal eigenvalues, experience squeezing, but the amount of squeezing applied to these modes is much less significant than the dominant mode. As the number of nodes N in the graph increases, the eigenvalue of the dominant mode also grows, indicating that a larger share of the squeezing resources is concentrated in this single mode. Meanwhile, the other modes have constant eigenvalues, regardless of the network's size. This consistency suggests that the squeezing applied to these modes doesn't change as the network expands. These modes reflect more balanced combinations of the quadratures across the network, where each node contributes similarly.
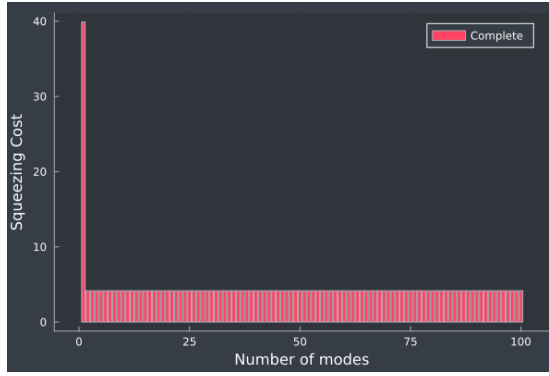
Figure 5.14: Squeezing spectrum of complete graph for 100 modes across squeezing cost in which modes in the horizontal direction and squeezing cost in the vertical direction

Linear Graph

In a line graph, the squeezing cost starts relatively high at the first mode due to boundary effects but decreases as move along the graph because the interior modes benefit from more balanced connections. By the time it reaches the hundredth mode pair, the system has evolved in such a way that the last mode requires no additional squeezing, resulting in a squeezing cost of zero.
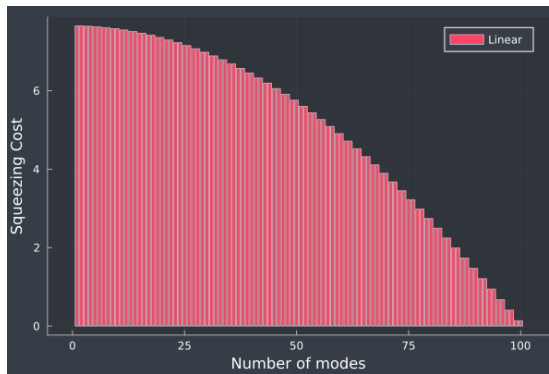

Figure 5.15: Squeezing spectrum of complete graph for 100 modes across squeezing cost in which modes on the x-axis and squeezing cost on the y-axis

Star Graph

In most network topologies, squeezing is distributed across all modes, with each mode receiving some level of squeezing to manage quantum noise. However, in a star network, the situation is different. Here, the squeezing is concentrated in just two modes: the central node and one of the peripheral nodes. This results in equal amounts of squeezing applied specifically to these two

modes. The peripheral nodes, lacking direct connections to each other, do not receive individual squeezing but are effectively included in the uniform squeezing applied to the central and one peripheral node. This unique distribution reflects the star network's structure, where the central node and its immediate connection are prioritized for squeezing, leading to a uniform squeezing effect in these initial modes.
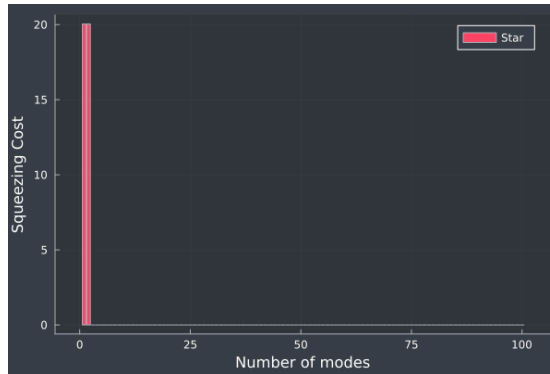

Figure 5.16: Squeezing spectrum of star graph for 100 modes across squeezing cost in which modes in the x-direction and squeezing cost in the y-direction

Wheel Graph

In a wheel graph, the squeezing is influenced by both the central hub and the rim nodes. The central hub plays a crucial role in the network, as it connects directly to all other nodes, influencing the overall squeezing distribution. In a wheel graph, the central hub node typically receives a substantial amount of squeezing due to its central role and connectivity to all other nodes. The rim nodes, arranged in a cycle and connected to the hub, experience a different squeezing distribution. The squeezing cost in the wheel graph is influenced by the combined effects of the central hub and the cyclic arrangement of the rim nodes, leading to a unique pattern of squeezing across the network.
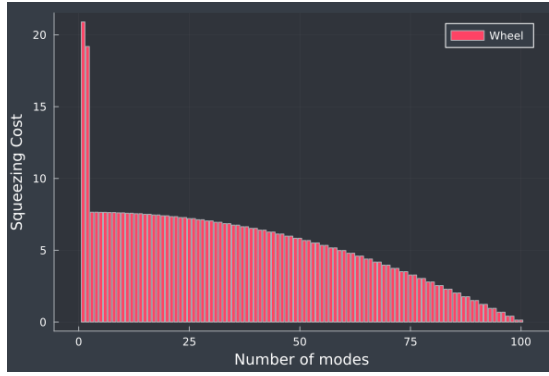
Figure 5.17: Squeezing spectrum of wheel graph for 100 modes across squeezing cost in which modes on the x-axis and squeezing cost on the y-axis

Grid Graph

In a grid graph, the squeezing cost starts higher due to the complex interconnections and noise management requirements across the network. As the number of modes increases, the squeezing cost decreases because the noise is distributed more evenly in a larger grid. By the time the number of modes reaches 100, the squeezing cost approaches a lower value, reflecting the efficient management of quantum noise in the expanded grid network. This pattern demonstrates how larger grid graphs can achieve more balanced and efficient squeezing as they scale.
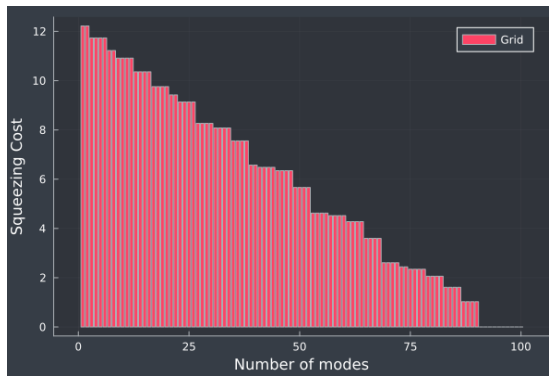

Figure 5.18: Squeezing spectra of grid graph for 100 modes across squeezing cost in which modes on the x-axis and squeezing cost on the y-axis

Cycle Graph

In a ring graph, the periodic boundary conditions imply that the first and last nodes are connected, creating a loop. This introduces small deviations in the squeezing spectrum compared to the linear graph, where the boundary effects are more pronounced because there are no di-

rect connections between the end nodes. As N increases, these deviations diminish because the influence of the boundary effects (in the linear graph) becomes less significant compared to the overall symmetry and connectivity of the large network. Essentially, with a large number of nodes, the difference between the boundary and interior nodes becomes less noticeable, and the squeezing spectra of the two types of graphs converge.
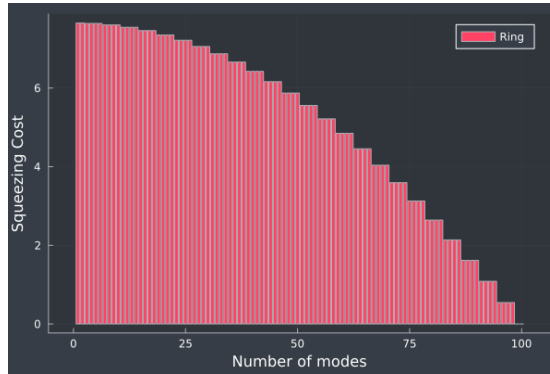

Figure 5.19: Graph plot for cycle graph for 100 modes across squeezing cost in which modes are horizontally and squeezing cost is vertically represented

All topoligies

Among the various network topologies, the complete graph exhibits the highest squeezing cost at the first mode, while all subsequent modes have significantly lower and equal squeezing costs. Both the path and cycle graphs share a similar squeezing spectrum, with a small variation; the squeezing cost starts at around 8 for the first mode and gradually decreases to zero by the last mode. In contrast, the star graph shows a high and equal squeezing cost for the first two modes, slightly below 20, with all other modes having a squeezing cost of zero. The wheel graph also begins with a high squeezing cost of around 20 for the first two modes, but the remaining modes follow a pattern similar to the cycle and path graphs. Lastly, the grid graph starts with a squeezing cost of approximately 12 at the first mode, which continuously decreases as the modes increase, eventually approaching a lower value by the 100th mode. Each topology thus reflects distinct squeezing cost behaviors, influenced by its unique structural characteristics.
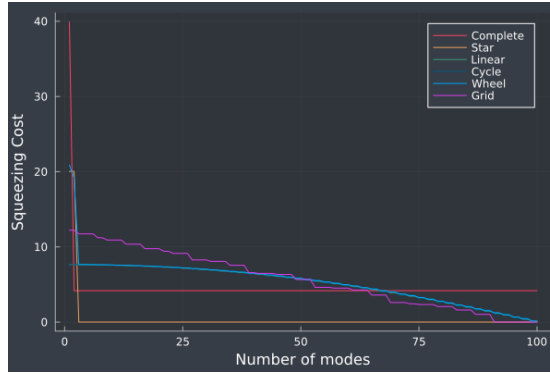
Figure 5.20: Trend of squeezing cost vs 100 modes of different networks in which red, yellow, green, bold green, blue, and purple represent the complete graph, star, path, wheel, cycle, and grid respectively

5.2 Squeesing cost with noise

The squeezing cost in a quantum network represents the resources required to maintain entanglement and quantum correlations across the network. When we introduce a beam splitter or noise, we effectively alter the transmission or interaction of quantum states between nodes. This can reduce the overall squeezing cost because the network may no longer need to maintain a high level of quantum correlation, thus requiring fewer resources.Hence,The reduction in squeezing cost reflects a decrease in the quantum resources needed.

5.2.1 For Nodes

Complete Graph

Every node is connected to every other node, creating a highly redundant network with many pathways for quantum information. When noise is added, it slightly disrupts the quantum correlations between some of these connections. However, due to the large number of redundant pathways, the network can still maintain its functionality without needing to use as much squeezing. The reduction from 453 to 452 reflects that the network is slightly less demanding in terms of resources when not all correlations need to be perfectly maintained. The overall structure remains robus, but with a marginally lower resource cost.
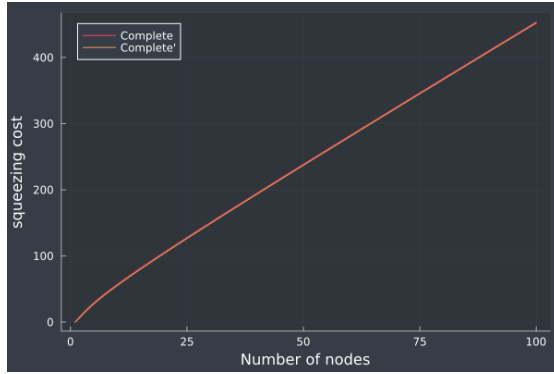
Figure 5.21: Graph plot for comparison of pure and lossy complete graph for 100 nodes in which red line shows pure network and yellow line shows lossy network.

Linear Graph

Nodes are connected in a straight line. In a path graph, quantum correlations must be maintained sequentially along the line. Introducing noise allows for a slight relaxation in these correlations, particularly between distant nodes, which reduces the squeezing resources needed. The decrease in squeezing cost represents the network's ability to handle a small amount of noise without significantly impacting its overall functionality.
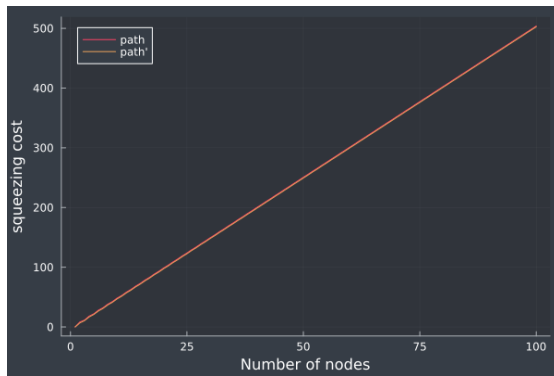

Figure 5.22: Graph plot for comparison of pure and lossy linea graph for 100 nodes in which red line shows pure network and yellow line shows lossy network

53

Cycle Graph

Each node is connected to two neighbors, forming a closed loop. Adding noise here slightly weakens the quantum correlations along the loop. Since the cycle graph has fewer connections than a complete graph, the impact of noise might be more pronounced, but the linear structure still allows the network to maintain its correlations with slightly reduced squeezing. The cost reduction from 506 to 505 shows that the network can tolerate a small amount of noise, leading to a minor decrease in the required resources.
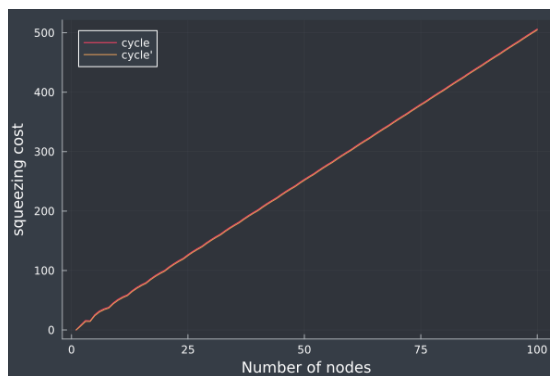

Figure 5.23: Graph plot for comparison of pure and lossy cycle graph for 100 nodes in which red line shows pure network and yellow line shows lossy network

Star Graph

All peripheral nodes are connected to a single central hub node. The central hub is crucial for maintaining correlations with all other nodes. Introducing noise might reduce the strictness of the correlations that need to be preserved, particularly between the hub and the peripheral nodes. This can ease the overall demand on squeezing resources because the hub doesn't need to maintain as perfect correlations with every node. The small reduction in squeezing cost indicates that the central hub can manage slightly less demanding correlations without losing network functionality.
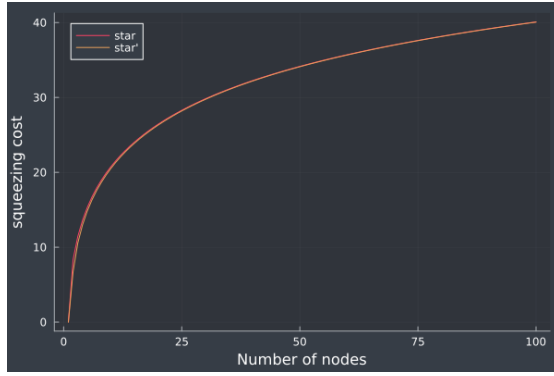
Figure 5.24: Graph plot for comparison of pure and lossy star graph for 100 nodes in which red line shows pure network and yellow line shows lossy network

Wheel Graph

A cycle graph with an additional central hub connected to all other nodes. Similar to the star and cycle graphs, noise reduces the strictness of the correlations required, both around the cycle and with the central hub. This mixed topology benefits from the central hub's ability to distribute quantum correlations, and noise slightly reduces the squeezing needed to maintain these correlations, especially in the cycle part of the wheel. The reduction in squeezing cost reflects this decrease in resource demand.

Figure 5.25: Graph plot for comparison of pure and lossy wheel graph for 100 nodes in which red line shows pure network and yellow line shows lossy network

Grid Graph

Nodes are arranged in a 2D lattice, where each node is typically connected to four neighbors. In a grid, maintaining quantum correlations over a larger number of nodes and edges becomes increasingly complex. Noise introduces some flexibility in these correlations, meaning the net-

work doesn't need to preserve as tight control over every edge, especially as the grid grows. The reduction in squeezing cost reflects that the grid can operate effectively with slightly lower resources as noise decreases the necessity for stringent correlations across all edges.
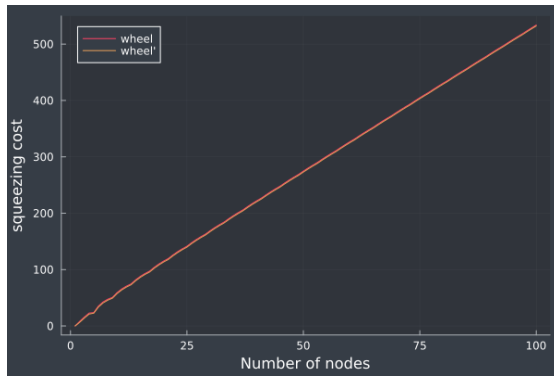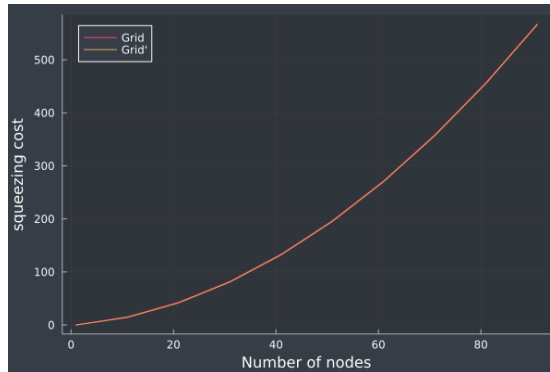

Figure 5.26: Graph plot for comparison of pure and lossy grid graph for 100 nodes in which red line shows pure network and yellow line shows lossy network

The decrease in squeezing cost when applying noise or a beam splitter can be interpreted as the network requiring slightly fewer quantum resources to maintain its functionality. This slight reduction happens because the noise decreases the level of quantum correlations that need to be preserved, allowing the network to operate with a slightly lower squeezing requirement. The effect is small, but it demonstrates how the network's resilience to noise can lead to a marginal reduction in resource demands across different topologies.

5.2.2 For Modes

When noise or a beam splitter is introduced into a quantum network, the squeezing cost decreases across all topologies. This reduction in squeezing cost can be explained by how noise and beam splitters affect the distribution and requirement of squeezing resources across the network's modes.

Complete Graph

In a complete graph, the dominant mode initially requires a significant amount of squeezing, with the other modes requiring much less. When noise or a beam splitter is added, the overall squeezing demand is reduced because the noise effectively introduces decoherence, which diminishes the quantum correlations between modes. As a result, the system's need for squeezing

56

to maintain those correlations decreases, leading to a lower squeezing cost across all modes, particularly in the dominant mode as shown in the figure
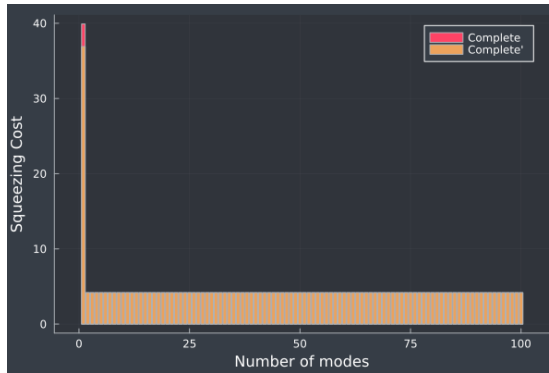

Figure 5.27: Graph plot for comparison of pure and lossy complete graph for 100 modes in which red line shows pure network and yellow line shows lossy network

Linear Graph

In a line graph, as shown in the figure, the squeezing cost is highest at the boundary modes and decreases along the interior modes. Introducing noise or a beam splitter smooths out the variations in squeezing requirements because the noise disrupts the sharp differences in mode correlations caused by boundary effects. This disruption reduces the overall squeezing cost, especially for the boundary modes, leading to a more uniform and lower squeezing requirement along the entire graph
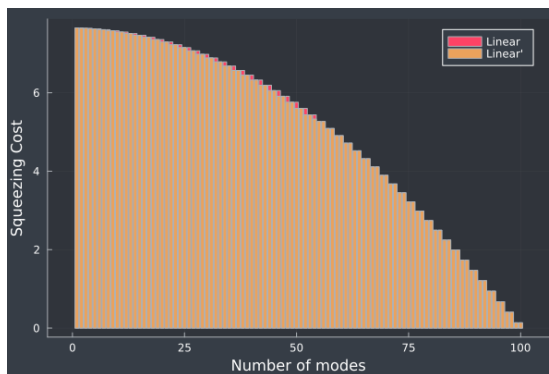

Figure 5.28: Graph plot for comparison of pure and lossy line graph for 100 modes in which red line shows pure network and yellow line shows lossy network.

Star Graph

In a star network, squeezing is concentrated in the central node and one peripheral node. When noise or a beam splitter is introduced, the central node's strong squeezing demand is reduced because the noise disperses the quantum correlations that create the need for concentrated squeezing as shown in the figure. This results in a decrease in the squeezing cost for the central and peripheral nodes, with the overall squeezing requirement across the network becoming more balanced and lower.
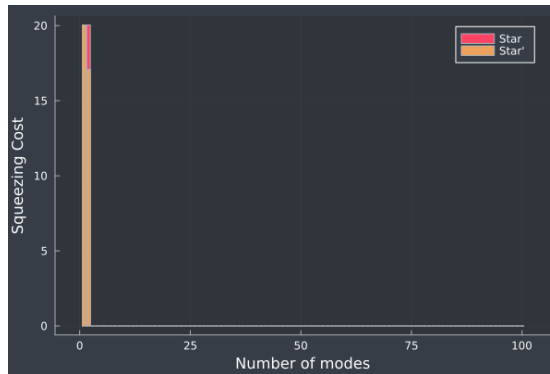

Figure 5.29: Squeezing Spectrum for comparison of pure and lossy star graph for 100 nodes in which red line shows pure network and yellow line shows lossy network

Cycle Graph

In the cycle graph shown in the figure below, the squeezing spectrum is affected by the loop structure, with some deviations compared to a line graph. When noise or a beam splitter is added, the squeezing cost decreases similarly to the line graph, but the reduction is more uniform due to the periodic boundary conditions. The noise disrupts the mode correlations evenly throughout the ring, leading to a lower squeezing cost across all modes. This effect results in a squeezing spectrum that becomes smoother and more uniform, further diminishing the differences between the cycle and line graphs.

Wheel Graph

In a wheel graph shown in the figure, the central hub and rim nodes each have distinct squeezing costs. Adding noise or a beam splitter reduces the squeezing demand on the central hub by disrupting the strong correlations between the hub and the rim nodes. As these correlations
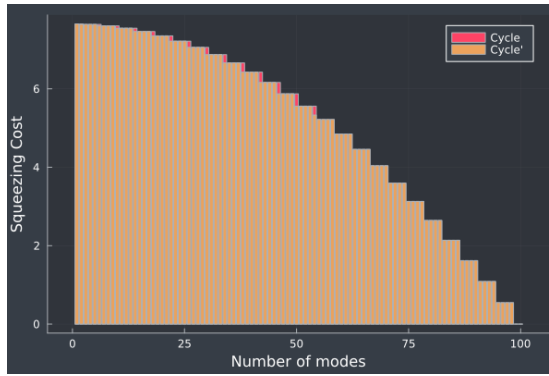
Figure 5.30: squeezing spectra for comparison of pure and lossy cycle graph for 100 nodes in which red line shows pure network and yellow line shows lossy network.

weaken, less squeezing is needed, leading to a decrease in the squeezing cost for both the hub and the rim nodes. This results in a more uniform and lower squeezing distribution across the wheel graph.

Figure 5.31: Graph plot for comparison of pure and lossy wheel graph for 100 nodes in which red line shows pure network and yellow line shows lossy network

Grid Graph

In a grid graph, the squeezing cost is initially high due to the complexity of the interconnections, but it decreases as the grid expands. Introducing noise or a beam splitter further reduces the squeezing requirement by spreading the noise across the network's interconnections as shown in figure. This reduction in squeezing cost occurs because the noise weakens the quantum

correlations that initially required high squeezing, leading to a more even and lower squeezing demand across the grid.
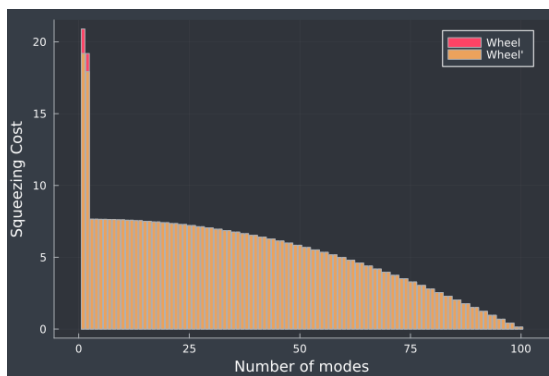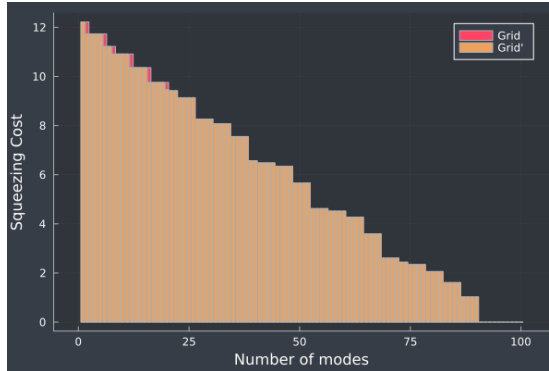

Figure 5.32: Graph plot for comparison of pure and lossy grid graph for 100 nodes in which red line shows pure network and yellow line shows lossy network.

Overall, the introduction of noise or a beam splitter reduces the squeezing cost in all network topologies by diminishing the quantum correlations that originally required high squeezing. This leads to a more uniform distribution of squeezing resources, with a generally lower squeezing cost across all modes, regardless of the network's structure. Each topology, however, experiences this reduction in squeezing cost in a way that reflects its unique structural characteristics, with some topologies (like the complete graph and star network) showing more pronounced decreases in specific modes.

Conclusion

We have explored the complex field of quantum information in this thesis, concentrating on continuous variables (CVs) and how they are used in quantum networks. We started by going over the fundamentals of quantum physics and comparing it with classical mechanics in order to highlight the special concepts of quantum systems like superposition and entanglement. This basic knowledge prepared the ground for an in-depth analysis of discrete variables (DVs) and qubits, defining them as the fundamental components of quantum information and emphasizing their role in quantum computation and communication.

The transition to continuous variables was then addressed, clarifying their advantages over discrete variables in certain quantum network contexts. We explored the conceptual framework of continuous variables and their associated quantum states, demonstrating their superiority in scenarios involving continuous measurement and high-dimensional encoding. This discussion was complemented by a thorough analysis of Gaussian states, including coherent states, displaced vacuum states, and squeezed vacuum states. The role of squeezing as a valuable resource was particularly emphasized, showing how it enhances measurement precision and information transfer within quantum networks.

Our investigation extended to the study of various quantum network topologies, such as linear, cycle, wheel, star, complete, and grid graphs. By quantifying the squeezing costs associated with these different network configurations, we uncovered how varying topologies impact the efficiency and resource requirements of quantum networks. Notably, our analysis of the effect of noise—through mechanisms such as beam splitters or varying transmissivity—revealed that noise can slightly reduce the squeezing cost in quantum networks. This insight is crucial for the practical design of quantum networks that can function effectively under realistic conditions.

Overall, this work significantly advances the understanding of continuous variables and their application in quantum networks. In summary, this thesis lays a solid foundation for the utilization of continuous variables in quantum networks and opens avenues for further advancements in the field.

.

Bibliography

[1] Rodney Loudon and Peter L Knight. "Squeezed light". In: *Journal of modern optics* 34.6-7 (1987), pp. 709–759.

[2] Nicolas J Cerf, Marc Levy, and Gilles Van Assche. "Quantum distribution of Gaussian keys using squeezed states". In: *Physical Review A* 63.5 (2001), p. 052311.

[3] Nicolas J Cerf, Marc Levy, and Gilles Van Assche. "Quantum distribution of Gaussian keys using squeezed states". In: *Physical Review A* 63.5 (2001), p. 052311.

[4] AS Daoud. "The variances in a single-mode superposed squeezed state". In: *Chinese Journal of Physics* 42.4 (2004), pp. 347–360.

[5] Alessio Serafini et al. "Entanglement and purity of two-mode Gaussian states in noisy channels". In: *Physical Review A* 69.2 (2004), p. 022318.

[6] Samuel L Braunstein and Peter Van Loock. "Quantum information with continuous variables". In: *Reviews of modern physics* 77.2 (2005), pp. 513–577.

[7] Samuel L Braunstein and Peter Van Loock. "Quantum information with continuous variables". In: *Reviews of modern physics* 77.2 (2005), pp. 513–577.

[8] Nicolas C Menicucci et al. "Universal quantum computation with continuous-variable cluster states". In: *Physical review letters* 97.11 (2006), p. 110501.

[9] Thaddeus D Ladd et al. "Quantum computers". In: *nature* 464.7285 (2010), pp. 45–53.

[10] Michael A Nielsen and Isaac L Chuang. *Quantum computation and quantum information.* Cambridge University Press, 2010.

[11] Matthew D Eisaman et al. "Invited review article: Single-photon sources and detectors". In: *Review of scientific instruments* 82.7 (2011).

[12]   Nicolas C Menicucci, Steven T Flammia, and Peter van Loock. "Graphical calculus for Gaussian pure states". In: *Physical Review A—Atomic, Molecular, and Optical Physics* 83.4 (2011), p. 042335.

[13]   Olivier Pinel et al. "Ultimate sensitivity of precision measurements with intense Gaussian quantum light: A multimodal approach". In: *Physical Review A—Atomic, Molecular, and Optical Physics* 85.1 (2012), p. 010101.

[14]   Christian Weedbrook et al. "Gaussian quantum information". In: *Reviews of Modern Physics* 84.2 (2012), pp. 621–669.

[15]   Gerardo Adesso, Sammy Ragy, and Antony R Lee. "Continuous variable quantum information: Gaussian states and beyond". In: *Open Systems & Information Dynamics* 21.01n02 (2014), p. 1440001.

[16]   Jonathan Roslund et al. "Wavelength-multiplexed quantum networks with ultrafast frequency combs". In: *Nature Photonics* 8.2 (2014), pp. 109–112.

[17]   Ulrik L Andersen et al. "Hybrid discrete-and continuous-variable quantum information". In: *Nature Physics* 11.9 (2015), pp. 713–719.

[18]   Bing Qi et al. "Generating the local oscillator "locally" in continuous-variable quantum key distribution based on coherent detection". In: *Physical Review X* 5.4 (2015), p. 041009.

[19]   Jaroslav Řeháček et al. "Surmounting intrinsic quantum-measurement uncertainties in Gaussian-state tomography with quadrature squeezing". In: *Scientific Reports* 5.1 (2015), p. 12289.

[20]   Daniel BS Soh et al. "Self-referenced continuous-variable quantum key distribution protocol". In: *Physical Review X* 5.4 (2015), p. 041010.

[21]   Martin Idel, Daniel Lercher, and Michael M Wolf. "An operational measure for squeezing". In: *Journal of Physics A: Mathematical and Theoretical* 49.44 (2016), p. 445304.

[22]   Yin Cai et al. "Multimode entanglement in reconfigurable graph states using optical frequency combs". In: *Nature communications* 8.1 (2017), p. 15645.

[23]   Alessio Serafini. *Quantum continuous variables: a primer of theoretical methods*. CRC press, 2017.

[24]   Manuel Gessner, Luca Pezzè, and Augusto Smerzi. "Sensitivity bounds for multiparameter quantum metrology". In: *Physical review letters* 121.13 (2018), p. 130503.

[25]   Fabian Laudenbach et al. "Continuous-variable quantum key distribution with Gaussian modulation—the theory of practical implementations". In: *Advanced Quantum Technologies* 1.1 (2018), p. 1800011.

[26]   Francesco Arzani et al. "Random coding for sharing bosonic quantum secrets". In: *Physical Review A* 100.2 (2019), p. 022303.

[27]   Claude Fabre and Nicolas Treps. "Modes and states in quantum optics". In: *Reviews of Modern Physics* 92.3 (2020), p. 035005.

[28]   Ludovico Lami, Ryuji Takagi, and Gerardo Adesso. "Assisted concentration of Gaussian resources". In: *Physical Review A* 101.5 (2020), p. 052305.

[29]   Bo-Han Wu et al. "Quantum computing with multidimensional continuous-variable cluster states in a scalable photonic platform". In: *Physical Review Research* 2.2 (2020), p. 023138.

[30]   Yun Shao et al. "Phase-reference-intensity attack on continuous-variable quantum key distribution with a local local oscillator". In: *Physical Review A* 105.3 (2022), p. 032601.

[31]   Federico Centrone, Frederic Grosshans, and Valentina Parigi. "Cost and routing of continuous-variable quantum networks". In: *Physical Review A* 108.4 (2023), p. 042615.

[32]   Mattia Walschaers et al. "Emergent complex quantum networks in continuous-variables non-Gaussian states". In: *Quantum Science and Technology* 8.3 (2023), p. 035009.